MOLECULAR ONCOLOGY 10 (2016) 1–23

available at www.sciencedirect.com

ScienceDirect

www.elsevier.com/locate/molonc

Determination of cell uptake pathways for tumor inhibitor lysyl oxidase propeptide☆

*Gokhan Baris Ozdener, Manish V. Bais, Philip C. Trackman**

Boston University, Department of Molecular and Cell Biology, Boston, MA 02118, United States

ARTICLE INFO

Article history:
Received 24 May 2015
Received in revised form
24 July 2015
Accepted 27 July 2015
Available online 6 August 2015

Keywords:
Lysyl oxidase
Propeptide
Macropinocytosis
Endocytosis
Tumor suppressor

ABSTRACT

The lysyl oxidase propeptide (LOX-PP) is derived from pro-lysyl oxidase (Pro-LOX) by extracellular biosynthetic proteolysis. LOX-PP inhibits breast and prostate cancer xenograft tumor growth and has tumor suppressor activity. Although, several intracellular targets and molecular mechanisms of action of LOX-PP have been identified, LOX-PP uptake pathways have not been reported. Here we demonstrate that the major uptake pathway for recombinant LOX-PP (rLOX-PP) is PI3K-dependent macropinocytosis in PWR-1E, PC3, SCC9, MDA-MB-231 cell lines. A secondary pathway appears to be dynamin- and caveola dependent. The ionic properties of highly basic rLOX-PP provide buffering capacity at both high and low pHs. We suggest that the buffering capacity of rLOX-PP, which serves to limit endosomal acidification, sustains PI3K-dependent macropinocytosis in endosomes which in turn is likely to facilitate LOX-PP endosomal escape into the cytoplasm and its observed interactions with cytoplasmic targets and nuclear uptake.

1. Introduction

Enzyme activity derived from all five lysyl oxidase family genes is required for the biosynthesis of connective tissues, while in cancer these enzymes promote metastatic disease (Barker et al., 2012). Evidence suggests that extracellular matrix modifications by lysyl oxidases promote metastasis by creating a permissive fibrotic extracellular environment (Ahn et al., 2013; Erler et al., 2009; Levental et al., 2009; Moreno-Bueno et al., 2011). The *LOX* gene, in addition, has tumor suppressor activity (Contente et al., 1990; Kenyon et al., 1991). The tumor suppressor activity originally attributed to LOX enzyme depends instead on the unique lysyl oxidase propeptide (LOX-PP) which is released from pro-lysyl oxidase by extracellular processing by procollagen C-proteinases (Palamakumbura et al., 2004). rLOX-PP is taken up by cells, and has RAS pathway intracellular targets, including RAF and HSP70 and nuclear targets, among others (Bais et al., 2015b; Sanchez-Morgan et al., 2011; Sato et al., 2011, 2013; Yu et al., 2012). The modes of rLOX-PP uptake are unknown, while the elucidation of rLOX-PP uptake pathways is expected to enhance the ability to design potential chemotherapeutics based on rLOX-PP structure.

Endocytic vesicles loaded with a substrate are subsequently closed and separated from the plasma membrane by dynamin- or actin-mediated mechanisms. Dynamin-dependent vesicles contain specific small GTPases and clathrin. By contrast, dynamin-independent vesicles, which

☆ Supported by NIH grants R21DE023973 and DOD W81XWH-08-1-0349 PC073646.
* *Corresponding author*. Boston University, Henry M. Goldman School of Dental Medicine, 700 Albany Street, W-201 Boston, MA 02118, United States. Tel.: +1 (617) 638 4076.
E-mail address: trackman@bu.edu (P.C. Trackman).
http://dx.doi.org/10.1016/j.molonc.2015.07.005

include macropinosomes and caveola-dependent vesicles, are closed by actin-mediated mechanisms (Khalil et al., 2006) (Figure 1). Actin-dependent uptake is a feature of macropinocytosis and is further classified as phosphatidylinositol 3-kinase (PI3K)-dependent or independent (Bar-Sagi and Feramisco, 1986; Bar-Sagi et al., 1987; Ellerbroek et al., 2004; Jimenez et al., 2000; Norbury, 2006; Porat-Shliom et al., 2008; Ridley et al., 1992; Sachdev et al., 2002). Cationic arginine rich peptides (CArPs) are taken-up by PI3K-dependent macropinocytosis which also depends on cell surface HSPGs (Sun et al., 2003). PI3K-dependent macropinocytosis is linked to RAC1-dependent lamellipodia formation which occurs in the invasive PC3 prostate cancer cell line (Araki et al., 2003; Kato et al., 2014). By contrast, PI3K-independent macropinocytosis is linked to CDC42 activation by growth factors and resulting filopodia formation (Royal et al., 2000) (Figure 1). Positively charged proteins can increase endosomal pH which leads to increased endosomal escape to other cytoplasmic targets by modulating the Na+/H+ antiport (Li et al., 1991; Nylander-Koski et al., 2006).

Cancer cells present multiple abnormalities in endocytic pathways. For example, enhanced internalization and unbalanced partitioning of internalized substrates between the lysosomal pathway and recycling, defects in the proteosomal system and malfunctioning of actin remodeling have all been described (Mosesson et al., 2008). Tumors with advanced survival characteristics can develop endocytosis-mediated defense systems against therapeutic agents. Anticancer therapeutic approaches could, therefore, potentially exploit macropinocytosis to deliver therapeutic agents to cancer cells (Commisso et al., 2013).

Here we report that the major pathway for rLOX-PP uptake is macropinocytosis in several cell lines. Data suggest that low endosomal pH enhances rLOX-PP uptake and that the buffering capacity of rLOX-PP can promote PI3K-mediated macropinocytosis. rLOX-PP can escape endosomes after uptake and thereby obtain access to its known intracellular targets and to the nucleus. This information will be useful in the design of rLOX-PP derivatives with enhanced or attenuated cell uptake and distribution.

2. Results

2.1. *LOX-PP inhibits human orthotopic oral cancer in mice*

rLOX-PP has been demonstrated to inhibit models of prostate and breast cancer growth in vitro and in vivo, and we have recently developed an orthotopic model of human oral cancer growth and metastasis in mice (Bais et al., 2015a). Here we first wished to determine whether ectopic expression of rLOX-PP could inhibit the growth and metastasis of UMSCC2 metastatic oral cancer cells implanted in mouse tongues. UMSCC2 oral cancer cells expressing DsRed were transduced with a lentivirus expression vector for rLOX-PP or empty vector. Cells were respectively injected into the tongues of nude mice at 500,000 cells per mouse. Caliper measurements were carried out at intervals and tumor volumes calculated. In vivo imaging of tumor cells in mice was conducted at intervals. Data (Figure 2) indicate that rLOX-PP expression inhibited both primary tumor growth and formation of metastases.

2.2. *Cellular uptake of rLOX-PP-Atto565*

Human breast, prostate and oral cancer cell lines and phenotypically normal osteoblasts are among the cell lines in which rLOX-PP has been shown to be biologically active (Bais et al., 2015b; Palamakumbura et al., 2009; Sanchez-Morgan et al., 2011; Sato et al., 2013; Vora et al., 2010b; Yu et al., 2012; Zhao et al., 2009). We, therefore evaluated uptake of rLOX-PP into cells representing this variety of cells. rLOX-PP was first labeled with Atto565 (Materials and methods section). rLOX-PP uptake was determined after incubation with cell lines for different time intervals, followed by flow cytometry. Increased rLOX-PP-Atto565 cell uptake occurred with time in both cancer cell lines and non-cancer cell lines (Figure 3A). Differences in uptake kinetics may suggest that uptake could occur by different pathways.

A subset of cell lines was then selected for further study and consisted of one non-cancer epithelial prostate cell line

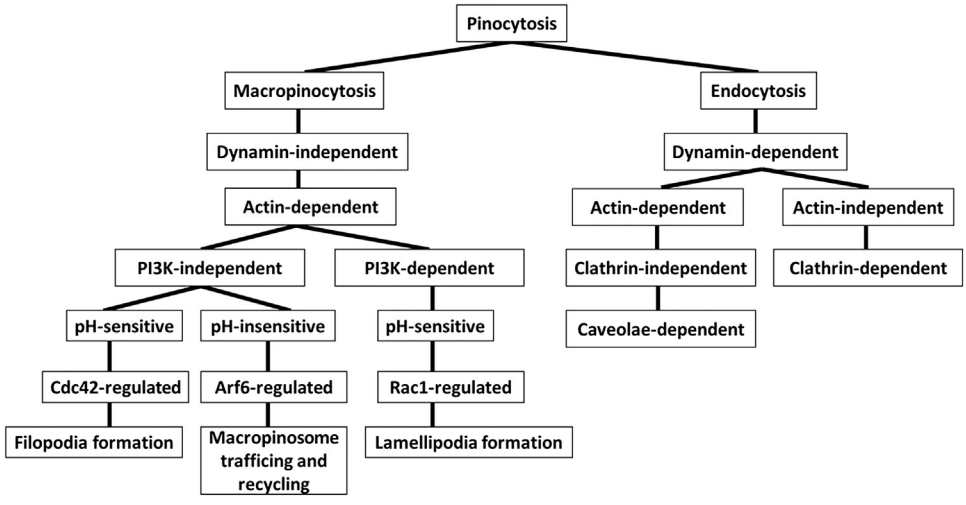

Figure 1 – Scheme for the pinocytosis pathways evaluated.

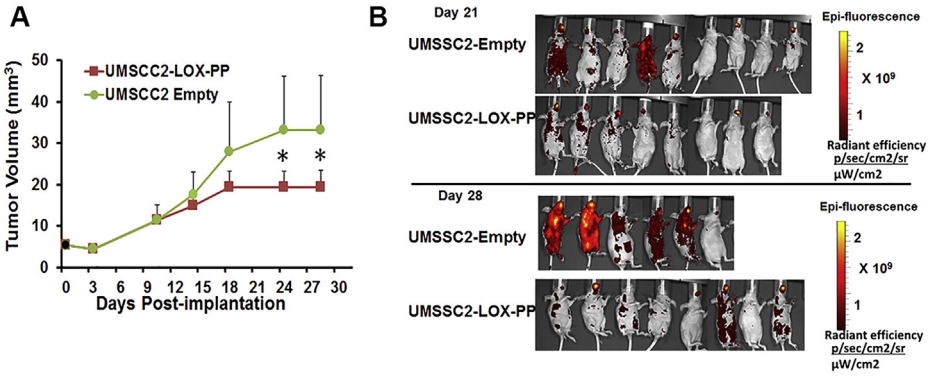

Figure 2 – rLOX-PP inhibits orthotopic growth and metastasis of human UMSCC2 oral cancer cells. UMSCC2 oral cancer cells expressing DsRed (Bais et al., 2015a) were transduced with a lentivirus expression vector for rLOX-PP (n = 8) or empty vector (n = 9). Cells were respectively orthotopically injected into nude mice at 500,000 cells per mouse. (A) Caliper measurements were carried out at intervals and tumor volumes calculated. (B) In vivo imaging of tumor cells in mice was conducted at intervals. Data indicate that rLOX-PP expression inhibited both primary tumor growth and formation of metastases. *p < 0.05, two way ANOVA with Bonferroni post hoc analysis.

(PWR-1E), two androgen-independent prostate cancer cell lines (DU145 and PC3), one non-invasive oral cancer cell line (SCC9) and one invasive breast cancer cell line (MDA-MB-231). Note that DU145 cells differ from PC3 cells in that the former creates osteoblastic bone lesions in mice, whereas PC3 cells are osteolytic (Zayzafoon et al., 2004). The functionality of rLOX-PP with and without Atto565 labeling was first compared by assessing the abilities of both proteins to inhibit FGF-2 dependent AKT activation in all cell lines. Data (Figure S1) indicate that both labeled and non-labeled rLOX-PP inhibited FGF-2 dependent AKT activation in PWR-1E and DU145 cells to the same degree, while no inhibition was observed in PC3 cells, as previously reported (Palamakumbura et al., 2009). Equivalent inhibition by labeled and non-labeled rLOX-PP was also observed in SCC9 cells, while no effect of either labeled or non-labeled rLOX-PP on AKT signaling was observed in MDA-MB-231 cells. Data suggest that Atto565 labeling of rLOX-PP does not interfere with activities of rLOX-PP given that the label is only present in the tag and at the N-terminus. Next, live cell imaging by confocal microscopy at 3 h of uptake further supported that rLOX-PP-Atto565 was taken up by these different cell lines (Figure 3B) which supports data in Figure 3A. This time point was selected because rLOX-PP-Atto565 fluorescence was

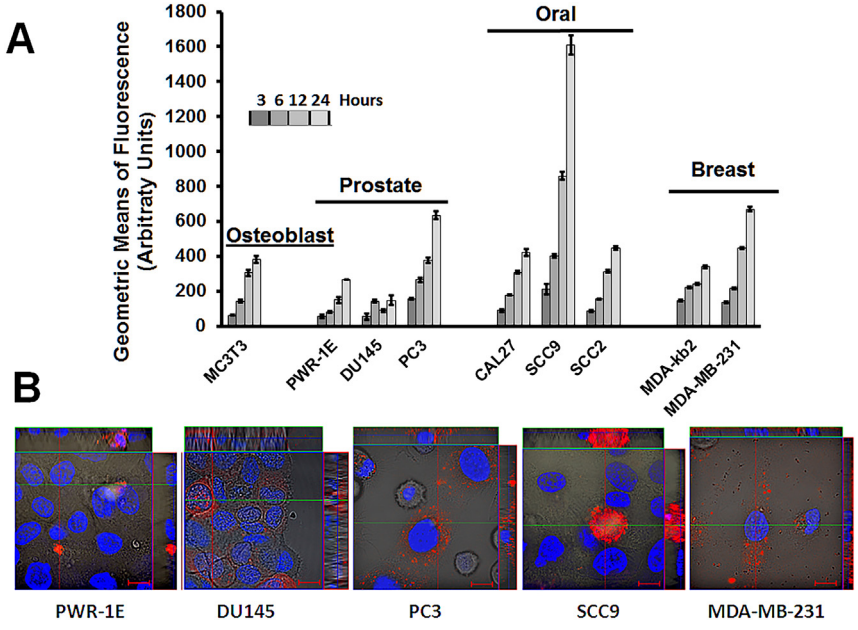

Figure 3 – Time-dependent cell uptake of rLOX-PP-Atto565 by a variety of cell lines. (A) Cell lines were incubated with 0.2 µM rLOX-PP-Atto565 and uptake was determined as a function of time by flow cytometry. Data are means of samples analyzed in triplicate ± SD, and experiments were performed at least twice. (B) Live cell imaging of selected cell lines by confocal microscopy after three hours further supports that rLOX-PP-Atto-565 (red) was internalized. Both cytoplasmic and apparent nuclear localization was observed. Nuclei were stained with Hoechst 33342.

easily observed, and because rLOX-PP-Atto565 remains intact under these conditions (Figure S2).

2.3. Dynamin-independent uptake of rLOX-PP

2.3.1. Actin-dependent rLOX-PP-Atto565 uptake

The high pI of rLOX-PP and its high arginine content (Vora et al., 2010a), suggests that that rLOX-PP could internalize into cells by macropinocytosis. Dextran (10 kDa) is taken up by cells via macropinocytosis, and co-localization of substrates with labeled 10 kDa dextran provides supporting evidence (Brabec et al., 2005; Foy et al., 2012; Krzyzaniak et al., 2013; Kwong et al., 2013; Malyukova et al., 2009; Rostaing et al., 2012). 0.2 μM rLOX-PP-Atto565 and 10 μM 10 kDa dextran-Bodipy-fl co-localization in cells was assessed by live cell imaging confocal microscopy. Figure 4 indicates that rLOX-PP-Atto565 and 10 kDa dextran-Bodipyfl fully or partially colocalized in all five cell lines.

Macropinocytosis and caveola-dependent uptake are actin-dependent, in contrast to dynamin and clathrin-uptake mechanisms which are actin-independent. Cytochalasins are actin polymerization inhibitors which attenuate macropinocytosis and caveola-dependent-uptake. All five cell lines were pretreated or remained untreated with cytochalasin D (1.5 μM) for 30 min, followed by rLOX-PP-Atto565 and flow cytometry. rLOX-PP-Atto565 uptake in the presence of cytochalasin D showed that the rLOX-PP-Atto565 uptake levels were inhibited in all five cell lines compared to controls (Figure 5A).

The effect on F-actin modification on rLOX-PP-Atto565 uptake in the presence or absence of cytochalasin D was visualized by confocal microscopy in SCC9 cells to independently establish that actin polymerization had been disrupted. Cells were treated as in Figure 5A, fixed, stained with Alexa 488-labeled phalloidin followed by Hoechst 33342 and cells imaged. rLOX-PP-Atto565 was surrounded by F-actin only in the absence of cytochalasin D. A high intensity actin ring surrounding large rLOX-PP-Atto565 clusters provides evidence for macropinosome formation that occurs around these large vacuoles. (Figure 5B1a–1b). Actin polymerization was diminished in the presence of cytochalasin D, as expected (Figure 5B-2). No loss of cell viability was observed (Figure 5C). Taken together, data strongly suggest that rLOX-PP-Atto565 is taken up by an actin-dependent pathway in all five cell lines.

2.3.2. PI3K-dependent macropinocytosis

PI3K dependency is a distinguishing feature of macropinocytosis. We next investigated PI3K involvement in rLOX-PP-Atto565 macropinocytosis. Inhibition of PI3K with LY294002 (100 μM) prevents closure of macropinocytotic cups (Araki et al., 1996). Therefore, the macropinocytotic cups remain open on the plasma membrane in the presence of LY294002. All five cell lines were pre-treated or remained non-treated with 100 μM LY294002 for 30 min, followed by rLOX-PP-Atto565 for 3 h, and flow cytometry. As shown in Figure 5D, treatment with rLOX-PP-Atto565 plus LY294002 for 3 h inhibited rLOX-PP-Atto565 uptake in all cell lines except

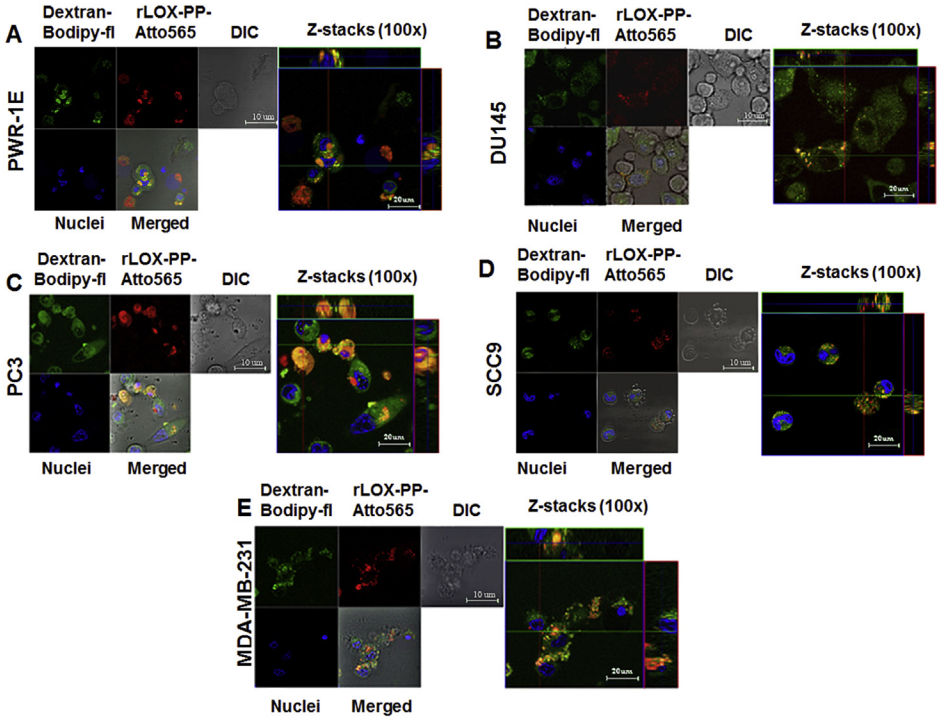

Figure 4 – Co-localization of rLOX-PP-Atto565 and 10 kDa dextran-Bodipy-fl. Cells were incubated with 10 μM 10 kDa dextran-Bodipy-fl (green) and 0.2 μM rLOX-PP-Atto565 (red) for 3 h before imaging by confocal microscopy. Confocal microscope images were formatted in split Z-stacks on the left and merged on the right for each cell line: (A) PWR-1E, (B) DU145, (C) PC3, (D) SCC9 and (E) MDA-MC-231. Corresponding dichromatic (DIC) images of cells are shown for each cell line.

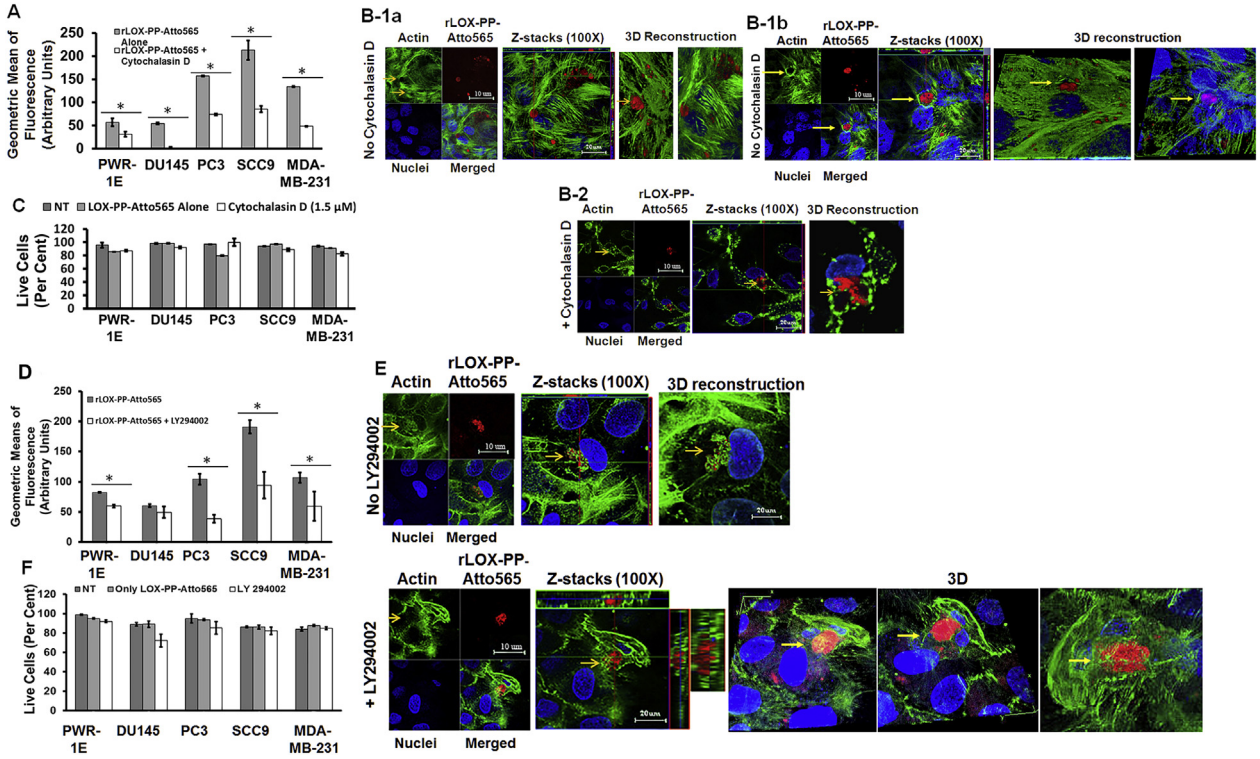

Figure 5 – Inhibition of rLOX-PP-Atto565 uptake in the presence or absence of cytochalasin D (A–C) or LY294002 (D–F). (A) After 3 h rLOX-PP-Atto565 uptake was quantified by flow cytometry in absence (grey) and presence of 1.5 μM cytochalasin D (white); n = 3; *, two-tailed p-value > 0.0002. SCC9 cells were pre-incubated on ice for 30 min in the absence (B-1a and B-1b) or presence (B-2) of cytochalasin D. rLOX-PP-Atto565 was added in the presence or absence of cytochalasin D for an additional 15 min on ice, and then incubated at 37 °C for 15 min in the 5% CO2 incubator. Cells were stained for F-actin (green) and DNA (blue) and indicate that 1.5 μM cytochalasin D disrupted actin filaments, as expected. Merged Z-series images of without cytochalasin (B-1a and B1b) and with cytochalasin D (B-2) treatment were reconstructed with the LSM image viewer software. (C) The LIVE/DEAD® Fixable Near-IR stain assay determined the percentage of live cells in each sample. (NT, dark gray bars; non treated control cells; rLOX-PP-Atto565, light gray bars; rLOX-PP-Atto565 + cytochalasin D, white bars). (D) rLOX-PP-Atto565 uptake was quantified by flow cytometry in the absence (gray bar) and in the presence of 100 μM LY294002 (white bar). Data are means ± SD; n = 3; *, two-tailed p-value > 0.0006. (E) SCC9 cells were treated with rLOX-PP-Atto565 (red) for 15 min and stained for F-actin (green) and DNA (blue) in absence and presence of 100 μM LY294002. Merged Z-series images of B without LY294002 (above) and with LY294002 (below) treatment were reconstructed with image J software. 3 dimensional images from various angles show cup formation that open to plasma membrane (F). The LIVE/DEAD® Fixable Near-IR stain assay was employed to determine the percentage of live cells in each cell lines; NT, dark gray bars, non-treated control cells; rLOX-PP-Atto565, light gray bars; LY294002 plus rLOX-PP-Atto565, white bars.

DU145. This result suggests that rLOX-PP-Atto565 uptake in these cell lines is PI3K-mediated macropinocytosis, with the possible exception of DU145 cells. We next sought to directly observe the effect on cup formation on rLOX-PP-Atto565 uptake in presence or absence of LY294002 by confocal microscopy. Data in Figure 5E indicate that treatment with LY294002 entrapped rLOX-PP-Atto565 in an immature macropinosome which opened to the cell surface in SCC9 cells (3D images from various angles). In contrast, rLOX-PP-Atto565 clusters appeared to be surrounded and packed by F-actin in the absence of LY294002. Cell viability was tested by flow cytometry and demonstrated no loss caused by rLOX-PP or LY294002 treatment (Figure 5F). Next, we evaluated the effect of endocytosis inhibitors on 10 μM 10 kDa dextran-Bodipy-fl uptake, a well-known macropinocytosis/fluid-phase uptake marker. Inhibition of 10 kDa dextran-Bodipy-fl was observed in all cell lines treated by 1.5 μM cytochalasin D for 3 h, as expected. LY294002 (200 μM) treatment significantly inhibited 10 kDa dextran-Bodipy-fl uptake in PWR-1E, PC3 and MDA-MB-231 cells. However, 100 μM dynasore did not reduce dextran uptake in any cell lines after 3 h as expected (Figure S3A). No loss of significant cell viability was observed (Figure S3B). Taken together, data strongly suggest that cytochalasin D is a selective inhibitor of actin-dependent uptake of 10 kDa dextran-Bodipy-fl, and that the dynamin inhibitor dynasore does not block macropinocytosis and caveola-dependent uptake, as expected.

2.4. *Dynamin-dependent uptake of rLOX-PP-Atto565*

The major pathway for the rLOX-PP-Atto565 uptake appears to by macropinocytosis in all cell lines with the possible exception of DU145. Macropinocytosis is a dynamin-independent uptake pathway in which formation and separation of macropinosomes from the plasma membrane is actin-dependent (Amyere et al., 2000; Araki et al., 2006; Hawkins et al., 1995;

Jiang and Chen, 2009; Damke et al., 1995 #21; Mercer, 2008 #14; Mercer and Helenius, 2009; Rossman et al., 2012). We wished to assess for any involvement of uptake mechanisms for rLOX-PP other than macropinocytosis. We therefore next determined if dynamin-dependent uptake of rLOX-PP occurred to any measurable degree in the cell lines of interest (Figure 1).

2.4.1. *Caveolae-mediated uptake for rLOX-PP-Atto565 internalization*

Ganglioside GM1-bound cholera toxin subunit B is taken up by cells via a caveolae- and clathrin-mediated pathway and serves as a marker for dynamin-dependent endocytosis (Montesano et al., 1982; Orlandi and Fishman, 1998; Parton et al., 1994; Shogomori and Futerman, 2001; Torgersen et al., 2001). Recombinant cholera toxin subunit B Alexa Fluor® 647 conjugate (CTxB-Alexa647) at a concentration of 7.5 μg/ml and 0.2 μM rLOX-PP-Atto565 were assessed for co-localization by confocal microscopy. rLOX-PP-Atto565 and CTxB-Alexa647 partially co-localized in PWR-1E, PC3 and MDA-MB-231 cell lines (Figure 6), suggesting that in these cell lines rLOX-PP uptake may be partially mediated by caveola. To further evaluate dynamin-dependent, caveola-mediated uptake of rLOX-PP-Atto565 caveola-dependence in these cell lines, CAV-1 expression was inhibited using siRNA. Knock-down cells were then subjected to uptake studies of rLOX-PP and CtxB-Alexa647. Loss of CAV-1 has been reported to result in defective caveolae-mediated-uptake (Li et al., 2013). Our data indicate that siRNA mediated knockdown of CAV-1 decreased levels of rLOX-PP-Atto565 uptake significantly in PC3 and MDA-MB-231 cells, increased uptake in SCC9 cells, while no effect of CAV-1 knockdown on uptake was observed in PWR-1E cells. In addition, CtxB-Alexa647 uptake was reduced by 50% or more by knockdown of CAV-1 (Figure 7A). No loss of significant cell viability was observed by used transfection protocol (Figure 7B).

Initiation of budding and internalization of ligands via caveolae-mediated uptake depend on transient phosphorylation of CAV-1 (Tiruppathi et al., 1997). CAV-1 phosphorylation is also crucial for the trafficking of ligands from early to late endosomes. For instance, depletion of CAV-1 and its constitutive phosphorylation results in the impaired intracellular trafficking of ligand-bound integrins and the increases in their recycling from early endosomes to the plasma membrane (Kozyulina et al., 2015). Therefore, to confirm the involvement of caveolae-mediated rLOX-PP-Atto565 uptake in cell lines, the relationship between CAV-1 phosphorylation levels on tyrosine residue 14 (pY14) and rLOX-PP-Atto565 uptake was analyzed in CAV-1 knockdown and control cells.

rLOX-PP treatment of control cells did not result in increased CAV-1 phosphorylation in PWR-1E, DU145 and SCC9 cells, but rLOX-PP increased CAV-1 phosphorylation in PC3 and MDA-MB-231 cells (Figure 8A). Thus, low rLOX-PP-Atto565 uptake in PC3 and MDA-MB-231 after CAV-1 knockdown, and the occurrence of transient CAV-1 phosphorylation in rLOX-PP-Atto565 treated PC3 and MDA-MB-231 indicate

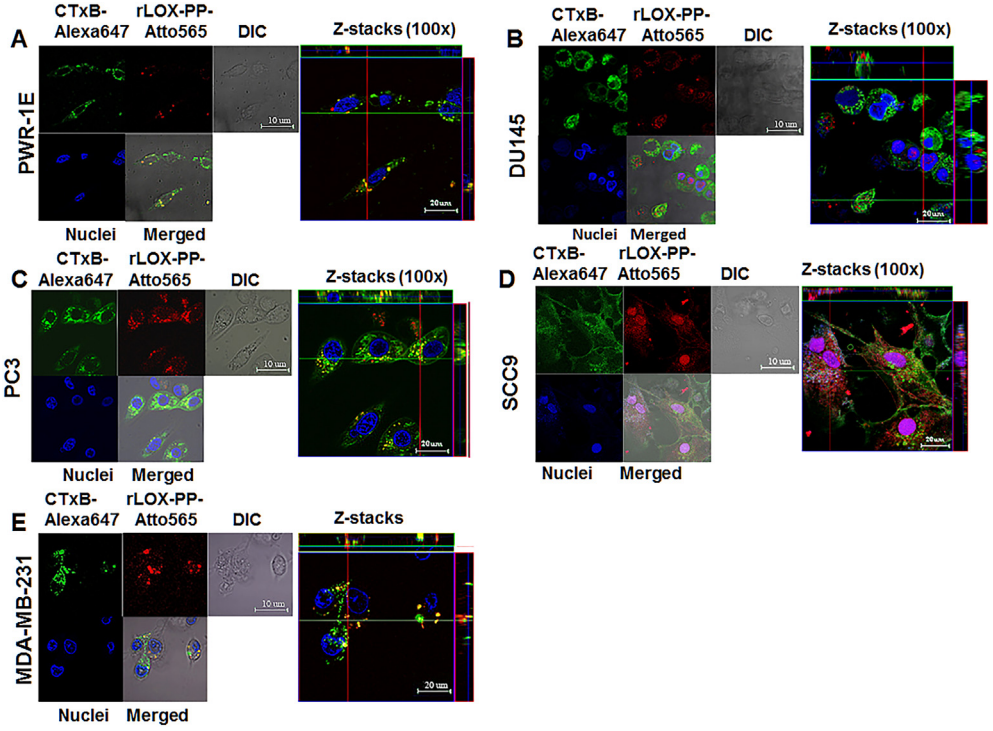

Figure 6 – Co-localization of rLOX-PP-Atto565 and CTxB-Alexa647 in various cell lines. Cells were incubated with CtxB-Alexa647 (652/668 nm-magenta) and rLOX-PP-Atto565 (563/592 nm-red) for 3 h before imaging. Confocal microscope pictures were formatted in split Z-stacks on the left and merged on the right for each cell line. PWR-1E (A), DU145 (B), PC3 (C), SCC9 (D) and MDA-MD-231(E) cell lines were listed; (DIC), dichromatic image of cells. Various levels of co-localization of rLOX-PP-Atto565 with CTxB-Alexa647 in PWR-1E, PC3, and MDA-MC-231 cell lines confirm that rLOX-PP-Atto565 enters the cell through a caveola-mediated pathway.

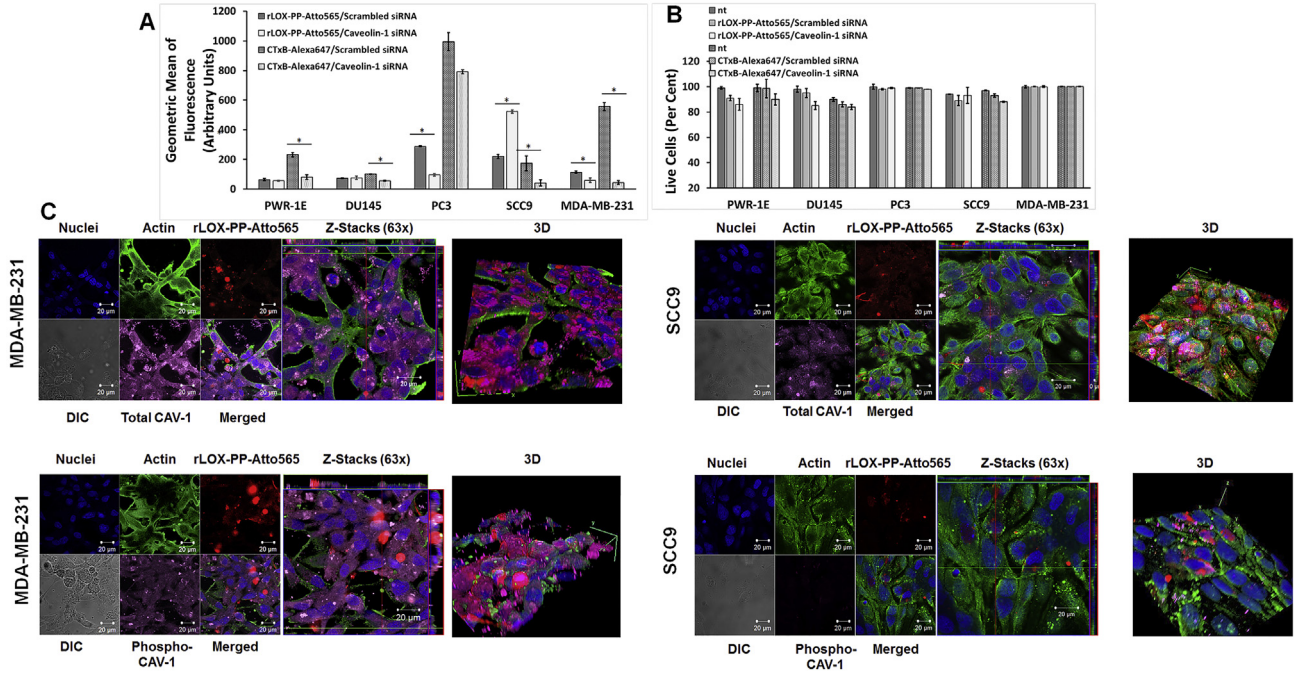

Figure 7 – Inhibition of caveolae-mediated rLOX-PP-Atto565 and CtxB-Alexa647 uptake by siRNA knockdown of the primary caveolae protein caveolin-1. (A) After transfection, cells were serum starved for 12 h followed by incubation with or without rLOX-PP-Atto565 or CtxB-Alexa647 for an additional 3 h rLOX-PP-Atto565 (solid gray and white) and CtxB-Alexa 647 (dashed gray and white) uptake were quantified by flow cytometry with (white) and without of CAV-1 knockdown (gray); Data are means ± SD, n = 3.; *, two-tailed p-value < 0.005 (B) The LIVE/DEAD® Fixable Near-IR stain assay was employed to determine the percentage of live cells in each sample. (NT, dark solid or dashed gray bars; non-treated control cells; rLOX-PP-Atto565 or CtxB-Alexa647, solid or dashed light gray bars; rLOX-PP-Atto565 or CtxB-Alexa647 + caveolin-1 siRNA knockdown, solid or dashed light white bars). Data are means ± SD, n = 3. (C) MDA-MB-231 (left) and SCC9 cells (right) were transfected with either caveolin-1 siRNA or control siRNA. 60 h after transfection, cells were serum starved for 12 h followed by incubation with or without rLOX-PP-Atto565 (red) for an additional 15 min on ice, and then incubated at 37 °C for 15 min in the 5% CO_2 incubator. Cells then were fixed, permeabilized and stained for F-actin (green), DNA (blue) and total caveolin-1 (magenta) or phospho caveolin-1 (magenta). Merged Z-series images with rLOX-PP-Atto565 (above) and without rLOX-PP-Atto565 (below) treatment were reconstructed with Zen Black Edition software. 3D images were constructed with Image J software.

that rLOX-PP-Atto565 uptake in these two cell lines is caveolin-dependent (Figure 8A).

To further analyze the differences of uptake kinetics of rLOX-PP-Atto565, serum starved, control or CAV-1 knocked down MDA-MB-231 and SCC9 cells, representing non-caveolae and macropinocytosis uptake, respectively, were visualized by confocal microscopy (Figure 8B). No CAV-1 phosphorylation was observed in either cell line in the absence of rLOX-PP-Atto565, while rLOX-PP induced a transient CAV-1 phosphorylation in MDA-MB-231 cells but not in SCC9 cells in the presence of rLOX-PP-Atto565. As expected, CAV-1 knockdown decreased rLOX-PP-Atto565 uptake in MDA-MB-231 cells, but increased CAV-1 independent rLOX-PP-Atto565 uptake in SCC9 cells. Interestingly, rLOX-PP-Atto565 distribution changed and appeared to accumulate in association with the plasma membrane of SCC9 cells.

While rLOX-PP-Atto565 uptake appeared to be caveola-dependent in cell lines in which rLOX-PP-Atto565 uptake was inhibited by CAV-1 knockdown, the loss of CAV-1 function in SCC9 cells increased rLOXPP-Atto565 uptake (Figure 7A). To further investigate this result, we directly observed total-and phospho-caveolin-1 level under same laser setup of the confocal microscope. It appears that the total caveolin-1 level is lower in SCC9 cells than MDA-MB-231 cells (Figure 7C). Moreover, rLOX-PP-Atto565 uptake did not trigger caveolin-1 phosphorylation in SCC9 cells while it did in MDA-MB-231 cells (Figure 8C). Taken together, these findings confirm the cavelolae-dependence of rLOX-PP uptake in MDA-MB-231 cells, and the cavelolae-independence of rLOX-PP uptake in SCC9 cells.

2.4.2. *Examination of clathrin-mediated uptake for rLOX-PP-Atto565*

Clathrin-mediated uptake is a dynamin-dependent receptor-mediated rapid uptake pathway (Figure 1). Uptake of transferrin is clathrin-mediated and labeled transferrin is a marker for this pathway (Huang et al., 2003; Thai et al., 2001). Live cells were treated with transferrin-FITC and rLOX-PP-Atto565 for 15 min on ice and then for 30 min at 37 °C, stained with Hoechst 33342 and imaged by live confocal microscopy (Rinne et al., 2007). Data indicate that rLOX-PP-Atto565 and transferrin-FITC partially colocalized in PC3 cells but did not significantly colocalize in the other cell lines tested (Figure 9). To further validate the finding of partial clathrin-

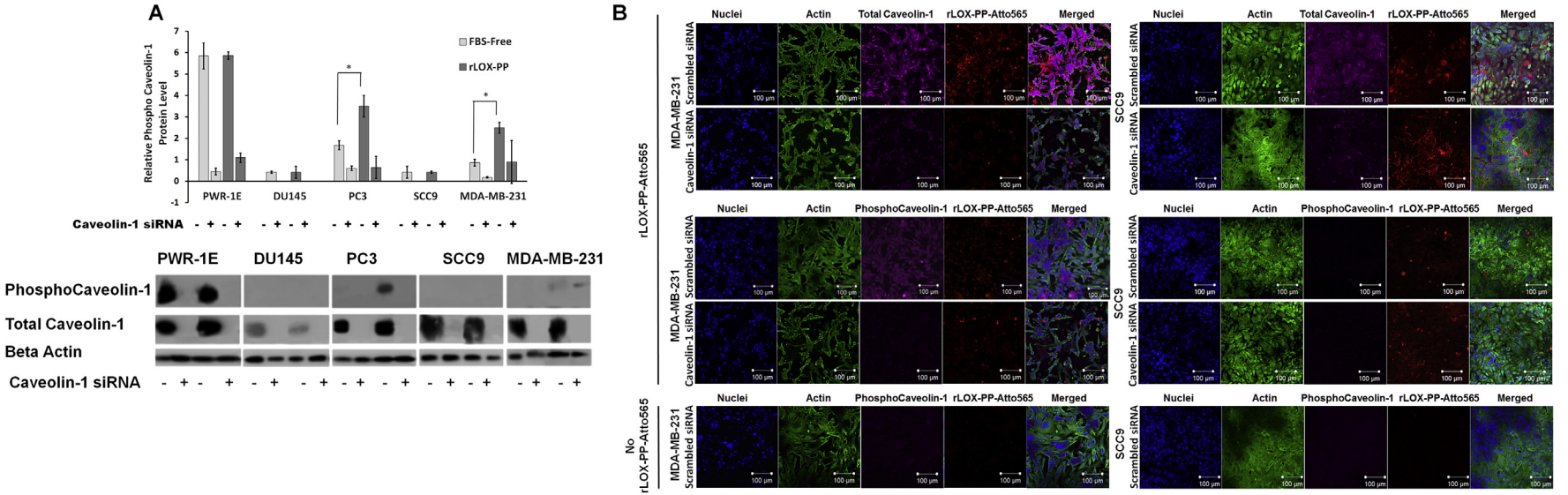

Figure 8 – siRNA knockdown of the caveolin-1 protein expression and the correlation of phospho caveolin-1 protein expression level in cells incubated in serum, serum starved or serum starved and rLOX-PP treated cells. (A) For confirmation of siRNA knockdown of the caveolin-1 protein, cells were transfected under similar conditions with either control (non-silencing) siRNA or siRNA directed against caveolin-1. Maximum reduction of caveolin-1 due to specific siRNA transfection was observed 75 h post-transfection. Sixty hours after transfection, cells were serum starved for 12 h followed by incubation with or without rLOX-PP for an additional 3 h. Cells extracts were subjected to SDS PAGE. Cell extract samples were probed with phosphor-caveolin-1, total caveolin-1 and band intensity against beta actin was quantified and relative phospho-CAV-1 protein expression was determined. This experiment was performed at least three times with the same outcomes. Data are means ± SD; n = 3; *, two-tailed p-value < 0.0001. (B) MDA-MB-231 (left) and SCC9 cells (right) were transfected with either CAV-1 siRNA or control siRNA. After transfection, cells were serum starved for 12 h followed by incubation with or without rLOX-PP-Atto565 (red) for an additional 15 min on ice, and then incubated at 37 °C for 15 min in the 5% CO_2 incubator. Cells then were fixed, permeabilized and stained for F-actin (green), DNA (blue) and total caveolin-1 (magenta) or –phospho caveolin-1 (magenta). Merged images with rLOX-PP-Atto565 (above) and without rLOX-PP-Atto565 (below) treatment were reconstructed with Zen Black Edition software.

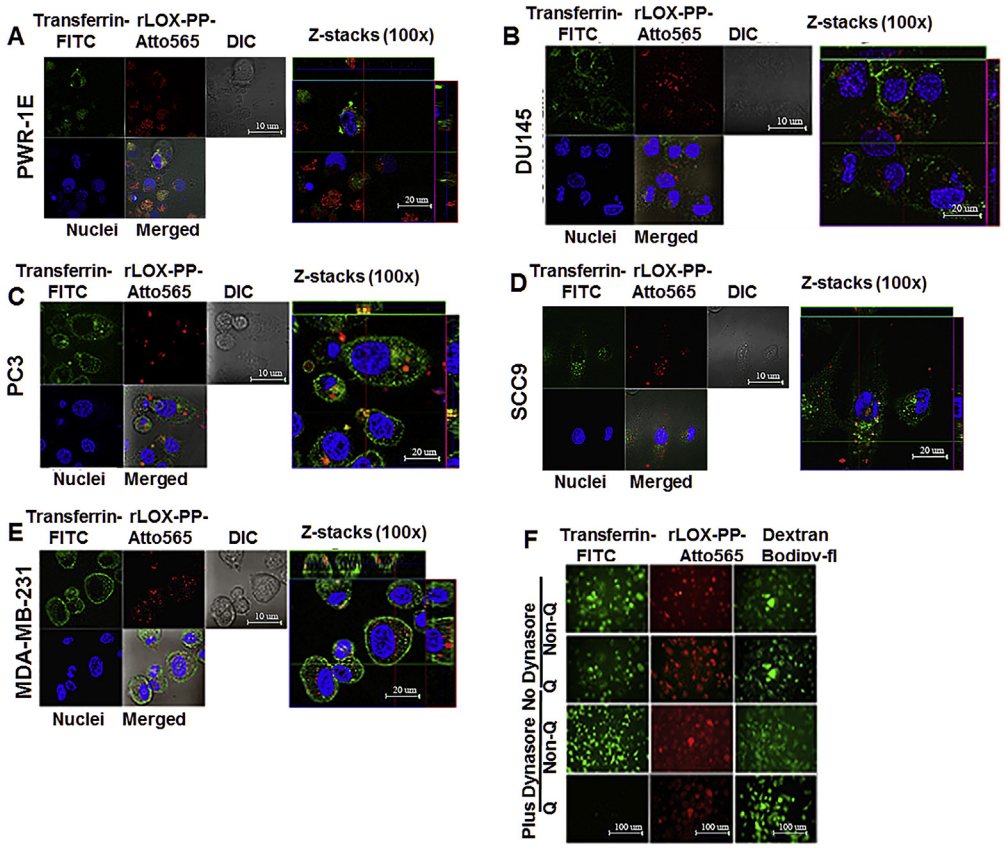

Figure 9 – Co-localization of rLOX-PP-Atto565 and transferrin-FITC in various cell lines and inhibition of rLOX-PP-Atto565 (A–E), and 10 kDa dextran-Bodipy-fl and transferrin-FITC uptake in presence or absence of dynasore in PC3 cells at 3 h (F). Cells were incubated with FITC-transferrin (green) and rLOX-PP-Atto565 (red) for 15 min on ice, and then 30 min at 37 °C before imaging. Nuclei were stained with Hoechst 33342 (blue). Confocal microscope images were formatted in split Z-stacks on the left and merged on the right for each cell lines. PWR-1E (A), DU145 (B), PC3 (C), SCC9 (D) and MDA-MC-231(E) cell lines were listed. Dichromatic (DIC) images are also shown. Transferrin (green) and rLOX-PP-Atto565 (red) co-localization was observed only in PC3 cells and confirms that rLOX-PP-Atto565 enters the PC3 cells through a clathrin-mediated pathway. In (F), uptake of transferrin-FITC was assessed after 30 min, while that of rLOX-PP-Atto565 and 10 kDa dextran-Bodipy-fl were assessed after three hours, in the presence or absence of dynasore in PC3 cells with or without quenching of extracellular fluorescence using a Zeiss Axiovert 100M inverted fluorescence microscope.

mediated uptake of rLOX-PP-Atto565 in PC3 cells, we treated PC3 cells with transferrin-FITC alone, rLOX-PP-Atto565 alone, or dextran-Bodipy-fl in the presence or absence of dynasore, which selectively targets dynamin- and clathrin-dependent uptake. As expected, total inhibition of transferrin-FITC-uptake, partial inhibition of rLOX-PP-Atto565 uptake and no inhibition of 10 kDa dextran-Bodipy-fl-uptake were observed in the presence of dynasore (Figure 9F). We conclude that rLOX-PP uptake into PC3 cells occurs partly by a clathrin- and dynamin-dependent pathway, while in all other cell lines tested rLOX-PP uptake is clathrin-independent.

Dynasore selectively targets dynamin- and clathrin-dependent uptake (Macia et al., 2006). We predicted that dynasore would inhibit LOX-PP uptake in PC3 cells only, and independently support the functional contribution of clathrin-mediated uptake in PC3 cells. Here, cells were pretreated or remained untreated with 100 μM dynasore for 30 min. Cell media were replaced with rLOX-PP-Atto565 containing media with or without 100 μM dynasore for 3 h, and analyzed by flow cytometry. Data show that treatment with dynasore decreased rLOX-PP-Atto565 uptake only in PC3 cells. Dynasore treatment increased rLOX-PP-Atto565 uptake in all other cell lines tested (Figure 10A). We conclude that while PC3 cells use macropinocytosis as a major pathway for rLOX-PP uptake, this cell line also uses a dynamin- and clathrin dependent uptake pathways for rLOX-PP uptake. We speculate that in the cell lines in which rLOX-PP-Atto565 uptake is increased by dynasore treatment, dynamin-independent uptake pathways may be up-regulated (see Discussion section) (Reyes–Reyes et al., 2010; Sandgren et al., 2010). Under the experimental conditions there was no loss of cell viability after dynasore treatment (Figure 10B).

Next, we wished to validate that selective pathway inhibitors used above actually selectively inhibit the intended endocytosis processes. We evaluated the effect of endocytosis inhibitors on uptake of 20 μM transferrin-FITC, a well-known clathrin-mediated uptake marker. Inhibition of transferrin-FITC was observed in all cell lines treated with 100 μM dynasore for 1 h (15 min at 4 °C and then 45 min at 37 °C). This is expected based on the ubiquitous expression and function

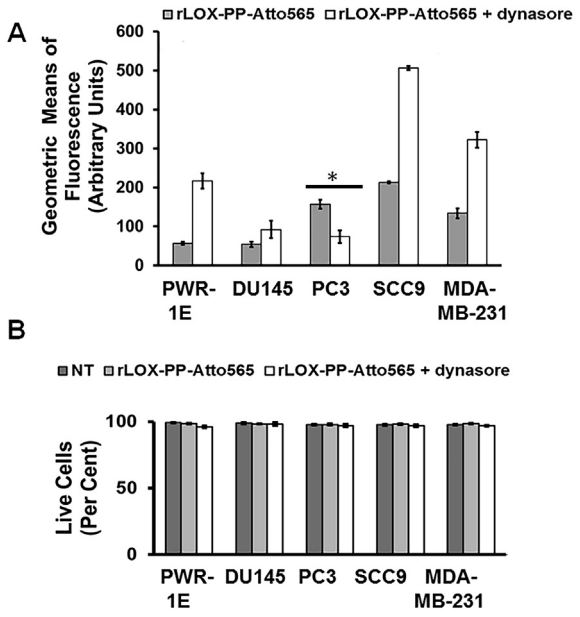

Figure 10 – Inhibition of clathrin-mediated uptake of rLOX-PP-Atto565 in presence or absence of dynasore. (A) After 3 h, rLOX-PP-Atto565 uptake quantified with flow cytometry in absence (gray bar) and presence of 100 μM dynasore (white bar); *, significant inhibition of uptake in PC3 cells only ($p < 0.000125$; $n = 3$). Up-regulation occurred in all other cell lines. (B) The LIVE/DEAD® Fixable Near-IR stain assay was employed to determine the percentage of live cells. NT (dark gray bars), non-treated control cells; rLOX-PP-Atto565 (light gray bars); rLOX-PP-Atto565 plus dynasore (white bars). Data are means ± SD, $n = 3$.

of the transferrin receptor. However, 1.5 μM cytochalasin D and 200 μM LY294002 treatment did not inhibit transferrin-FITC uptake also as expected because these inhibitors are effective at inhibiting macropinocytosis which is not employed by transferrin (Figure S3C). No loss of significant cell viability was observed (Figure S3D). Taken together, data from this control experiment support that the combination of the cells studied and inhibitors employed above appropriately and selectively target respective uptake pathways.

2.5. *Evaluation of intracellular pH (pHi) modification caused by rLOX-PP uptake*

As noted, LOX-PP is a highly basic protein and this feature of LOX-PP could contribute to its uptake. To first directly assess this hypothesis intracellular pH was modulated with EIPA, and bafilomycin A1, respectively, and rLOX-PP-Atto565 uptake was determined. EIPA is an inhibitor of the Na^+/H^+ pump on plasma membranes and inhibits macropinocytosis (Rothenberg et al., 1983). Actin-remodeling throughout macropinocytosis depends on the activation of pH sensitive GTPases. Inhibition of the Na^+/H^+ pump by EIPA on plasma membranes lowers macropinosome pH and inhibits Rac1/Cdc42 GTPase activation (Gerbal-Chaloin et al., 2007; Koivusalo et al., 2010). On the other hand, bafilomycin A1 is a specific inhibitor of vacuolar ATPases on the plasma membrane and endosomes. Bafilomycin A1 prevents maturation of early- and late endosomes and lysosomes at nanomolar concentrations by inhibiting endosomal acidification after scission of endosomes from the plasma membrane (DePedro and Urayama, 2009; Drose and Altendorf, 1997; Fischer et al., 2004; Tapper and Sundler, 1995; Yoshimori et al., 1991).

Cells were treated either with or without 100 μM EIPA or 1 μM bafilomycin A1 for 30 min followed by rLOX-PP-Atto565 for 3 h and uptake levels were compared by flow cytometry. Data show that bafilomycin A1, which causes the loss of acidification of endosomes, decreased rLOX-PP-Atto565 uptake levels in all cell lines (Figure 11A). However, EIPA which causes acidification of macropinosomes, increased rLOX-PP-Atto565 uptake (Figure 11B). Cell viability was tested by flow cytometry and demonstrated that there was no loss after bafilomycin A1 or EIPA treatment (Figure 11C and D).

We next evaluated whether increased rLOX-PP uptake in EIPA treated cells may be caused by rLOX-PP itself as a result of its high isoelectric point. Although decreased endosomal pH can inhibit uptake and endosomal delivery of some ligands, positively charged ligands such as epidermal growth factor (EGF), may increase endosomal pH after internalization, resulting in endosomal escape and distribution to other cytoplasmic targets, increasing total uptake (Li et al., 1991; Nylander-Koski et al., 2006). To evaluate whether rLOX-PP can change the endosomal pH through its uptake, in situ pH measurement experiments were employed using the fluorescent pH indicator and Lysosensor Yellow/Blue dextran to determine the in situ endosomal pH and simultaneously track rLOX-PP localization. Based on time points and size determination of endosomes, dextrans labeled with pH sensitive fluorescent probes are useful tools to measure pH of endosomal and macropinosomal organelles because dextrans accumulate in endosomes (Lin et al., 2003; Nowak-Lovato et al., 2010; Wang et al., 2014).

When Lysosensor Yellow/Blue labeled dextran is excited at its excitation isobestic point (360 nm), its emission shifts to longer wavelengths in acidic environments. It has an emission isobestic point (490 nm) used to calibrate the fluorescent intensity of samples at various pH values. The ratio of fluorescence at lower and higher wavelengths from its emission isobestic point can be used to measure intracellular pH (Bonanno and Giasson, 1992; Lin et al., 2001).

SCC9 cells were first treated with 2 μM Lysosensor Yellow/Blue dextran alone for 3 h and fluorescence emissions were recorded in pH in calibration buffers to generate a calibration curve (Figure S4). Atto647N was selected to label rLOX-PP to avoid unwanted FRET and fluorescence bleeding between Lysosensor Yellow/Blue dextran and Atto565. In the experimental samples, cells were treated with bafilomycin A1 or EIPA or remained untreated for 30 min. Cells were then exposed to rLOX-PP-Atto647N-, EIPA-, or bafilomycin A alone; or with rLOX-PP-Atto647N plus EIPA; or rLOX-PP-Atto647N plus bafilomycin A1 for 3 h; or were untreated; all in presence of 2 μM Lysosensor Yellow/Blue dextran. SCC9 cells were chosen for this experiment because rLOX-PP uptake was fully dependent on macropinocytosis, and the level of rLOX-PP uptake is the highest in this cell line compared to the others used in this study (Figure 3). Findings indicate that rLOX-PP-Atto647N totally co-localized with macropinosome marker Lysosensor Yellow/Blue dextran, as expected. Most important, a pH modulation effect of rLOX-PP was clearly observed (Figure 12). rLOX-PP-

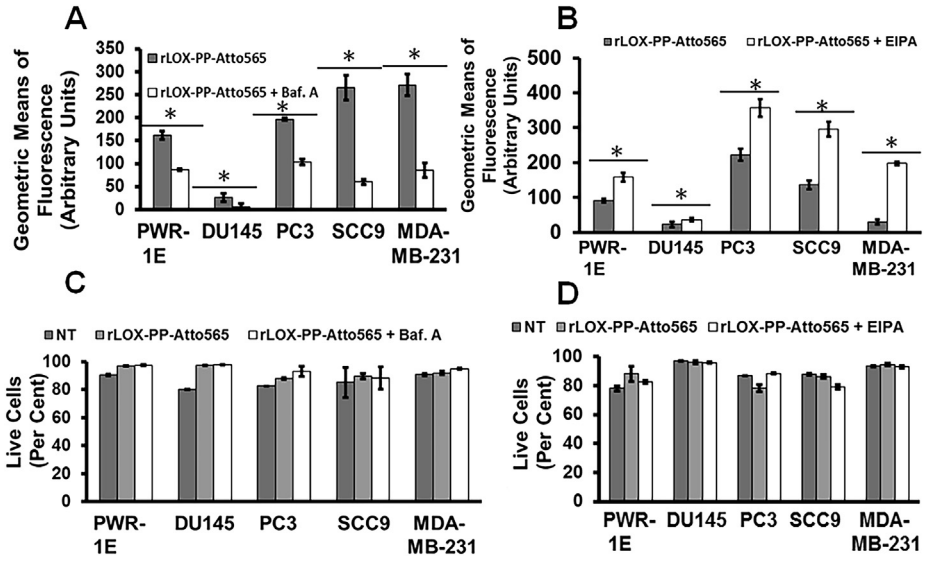

Figure 11 – rLOX-PP-Atto565 uptake in bafilomycin A1 and EIPA treated cells. Cells were pre-treated in the presence or absence of bafilomycin A1 (A) or EIPA (B), and rLOX-PP-Atto-565 uptake was measured by flow cytometry after 30 min of incubation. Bafilomycin decreased rLOX-PP-Atto565 uptake after 30 min. Data are means ± SD, n = 3; *, $p < 0.005$. rLOX-PP uptake was inhibited by bafilomycin A, while it was stimulated by EIPA in all cell lines except possibly DU145 cells. In C and D, the LIVE/DEAD® Fixable Near-IR stain flow cytometry assay was used to determine the percentage of live cells. NT (dark gray bars), non-treated control cells; rLOX-PP-Atto565 (light gray bars), bafilomycin A- or EIPA- + rLOX-PP-Atto565 (white bars).

Atto647N reversed the pH lowering effect of EIPA alone, and resulted in an increased endosomal pH in Lysosensor Yellow/Blue dextran loaded endosomes (Figure 12A and 12B). In the presence of EIPA, the alkalinizing effect of rLOX-PP-Atto647N on the pH drop was greater than the alkalinizing effect of bafilomycin A1 (Figure 12B). It was observed that rLOX-PP-Atto647N increased endosomal pH from 6.77 to 6.85 in SCC9 cells (Figure 12B). We conclude that protonization of basic residues of rLOX-PP-Atto565 may increase endosomal pH by enhancing the function of the Na+/H+ antiporter similar to effects reported for EGF (Li et al., 1991; Nylander-Koski et al., 2006). Increased uptake of rLOX-PP-Atto565 measured by flow cytometry in EIPA treated cells correlates well with increased pH of macropinosomes and early endosomes. This raises the possibility that pH modulation by rLOX-PP may enhance its own retention and accumulation in endosomes.

To independently investigate whether the electrostatic charge of rLOX-PP-Atto565 influences its uptake, its isoelectric point was increased by removal of the $(His)_6$-tag. Based on its substrate specificity carboxypeptidase A can remove the last 12 residues of the myc-$(His)_6$ tag of rLOX-PP while preserving the lysine residue contained in the myc tag used for labeling with NHS-activated Atto-565 (Waugh, 2011). Theoretical calculations with PROTEIN CALCULATOR v3.3 software (Joshi et al., 2012), indicate that $(His)_6$-tag removal up to the lysine residue increases the pI of rLOX-PP-Atto565 from 11.30 to 11.68, and increases its charge from +8.40 to +10.10 at pH 7.15 which occurs in the SCC9 extracellular environment. Upon macropinosome entry at pH 6.77, the charge of rLOX-PP-Atto565 containing the $(His)_6$ tag would decrease to +9.90, and endosomal pH would increase to 6.85. By contrast, removal of $(His)_6$-tag from rLOX-PP-Atto565 and endosomal entry at pH 6.77 would result in a charge of +10.30. Thus, the effect of the removal of the $(His)_6$-tag rLOX-PP-Atto565 was assessed in DU145 and PC3 cells after 3 h of exposure at the same concentrations. Data indicate that $(His)_6$-tag removal increased rLOX-PP-Atto565 uptake in both cell lines (Figure 13A). Furthermore, pretreatment with non-labeled rLOX-PP decreased rLOX-PP-Atto565 in all cell lines. We suggest that similar to bafilomycin A1 treatment, alkalization of endosomes by rLOX-PP pretreatment decreased its own uptake (Figure 13B). Data in Figures 11, 12 and 13 suggest that optimum rLOX-PP internalization into cells appears to require endosome acidification.

3. Discussion

rLOX-PP is a naturally occurring cationic protein with tumor inhibiting properties and has the potential to provide a basis for the development of novel cancer therapeutics. Although, some intracellular targets and molecular mechanisms of rLOX-PP have been identified, some of its tumor inhibiting properties may occur on the cell surface (Sanchez-Morgan et al., 2011; Vora et al., 2010b). Understanding and elucidating cell uptake of rLOX-PP by a variety of different cell lines will help us to understand and manipulate the degree to which it is taken up. This information will help to establish its primary functional sites of action and will inform future strategies for developing formulations for the potential use of rLOX-PP or a derivative as a cancer therapeutic.

3.1. *Macropinocytosis of rLOX-PP-Atto565 as a major uptake pathway*

Data demonstrated that rLOX-PP-Atto565 enters cells primarily by macropinocytosis in all cell lines tested based on its co-

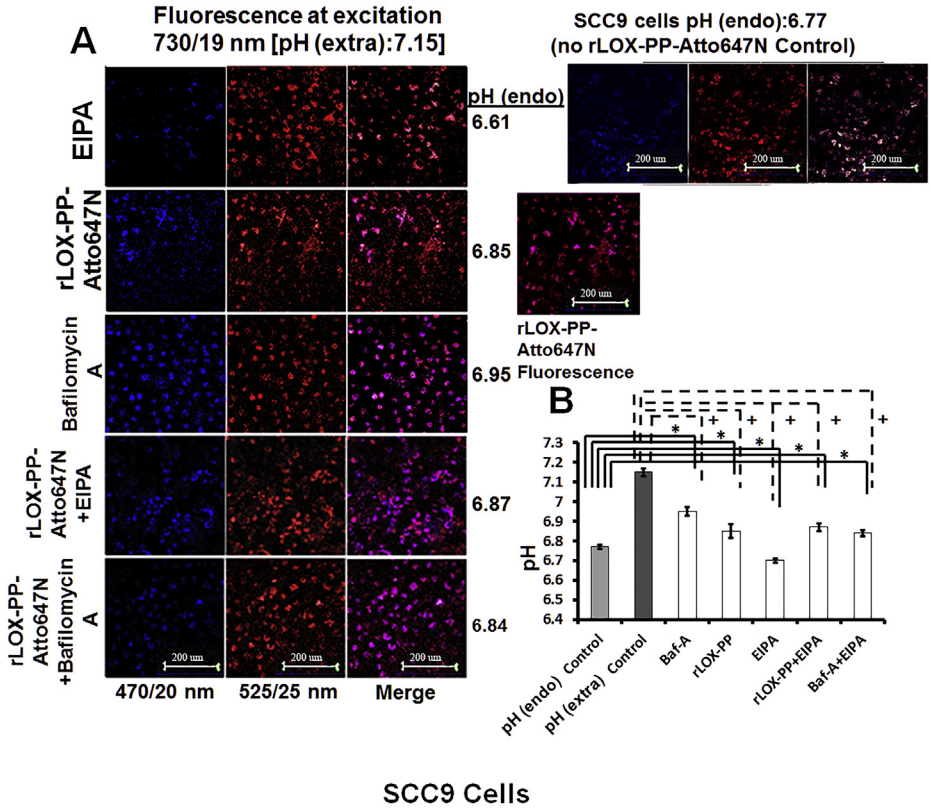

Figure 12 – Internalized rLOXPP-Atto647N increased endosomal pH from 6.77 to 6.85. In (A), SCC9 cells were maintained in the recording buffer at pH 7.15 for steady state extracellular pH and incubated with Lysosensor Yellow/Blue dextran ± rLOX-PP-Atto647 and/or EIPA or bafilomycin A for 3 h. Images were obtained by confocal microscopy with a 20x objective and Lysosensor Yellow/Blue dextran emission was collected in 470 ± 20, 490 ± 10 and 525 ± 25 nm band ranges. 470 ± 20 and 525 ± 25 nm were artificially colored as blue and red consecutively. 470 ± 20 (blue) and 525 ± 25 (red) emission ratios were compared with the calibration curve. 675 nm and higher rLOX-PP-Atto647N emission was collected and artificially colored as magenta. (Artificially magenta colored emission integral of rLOX-PP-Atto647N was collected to avoid overlap between Yellow/Blue dextran 10,000 and rLOX-PP-Atto647N emission in rLOX-PP-Atto647N treated samples). In rLOX-PP-Atto647N treated cells, the merged image on the right side shows that rLOX-PP-Atto647N and Lysosensor Yellow/Blue dextran 10,000 MW co-localize. Images show endosomal pH (pH endo) measurements which change as a function of either rLOX-PP-Atto647N bafilomycin A1, EIPA and combinations in SCC9 cells (images were collected with EC-Plan Neofluar 40x/1.30 oil DIC M27 objective). The excitation wavelength was 740 nm (two photon), and emission was detected in 4 channels: 470/20, 490/10 and 525/25 nm for Lysosensor Yellow/Blue dextran 10,000 MW, and 669/25 nm for rLOX-PP-Atto647N. In (B), SCC9 cells were treated with either both rLOX-PP-Atto647N and EIPA or bafilomycin A1 and EIPA to assess whether rLOX-PP-Atto647N or bafilomycin A1 can reverse the endosomal pH drop caused by EIPA treatment.

localization with the macropinocytosis tracker 10 kDa dextran-Bodipy-fl, and effects of actin disruption on uptake. Evidence supporting the PI3K-subtype of macropinocytosis of rLOX-PP-Atto565 was further obtained after assessing effects of LY294002 on uptake. Rac1 promotes macropinocytosis downstream of PI3K. LY294002 also inhibits Rac1 activity (Mercer and Helenius, 2009; O'Connor et al., 2012; Paulucci-Holthauzen et al., 2009). The relative importance of PI3K and Rac1 in mediating macropinocytosis or rLOX-PP is currently unclear. Inhibition of LOX-PP uptake by LY294002 in all cell lines tested except possibly DU145 cells is consistent with this occurring by macropinocytosis. Unlike other cell lines tested, rLOX-PP-Atto565 uptake in DU145 cells was actin-dependent and caveolae/clathrin-independent. While DU145 and PC3 cells are both androgen-independent prostate cancer cell lines, they are phenotypically and functionally different cell lines. DU145 cells produce osteoblastic lesions, while PC3 cells produced osteolytic bone lesions (Fradet et al., 2013; Zayzafoon et al., 2004). Similarly, data support that rLOX-PP-Atto565 uptake in DU145 cells occurs by a pH sensitive, Cdc42-dependent but Rac1-independent form of macropinocytosis while rLOX-PP-Atto565 uptake in PC3 cells occurs by PI3K-dependent macropinocytosis (Fujii et al., 2013; Redelman-Sidi et al., 2013).

Macropinosomes are relatively large endosomes with no coat (Conner and Schmid, 2003). These leaky vacuolar membranes can be exploited to provide cellular entry routes to deliver macromolecules into the cytoplasm (Zouwail et al., 2005). Uptake and distribution of the HIV TAT peptide and of octaarginine occurs by macropinocytosis (Heitz et al., 2009; Kaplan et al., 2005; Nakase et al., 2004, 2007; Wadia et al., 2004). Uptake of rLOX-PP by macropinocytosis in cancer cells is consistent with our observation that rLOX-PP has been found to associate with cytoplasmic and nuclear proteins

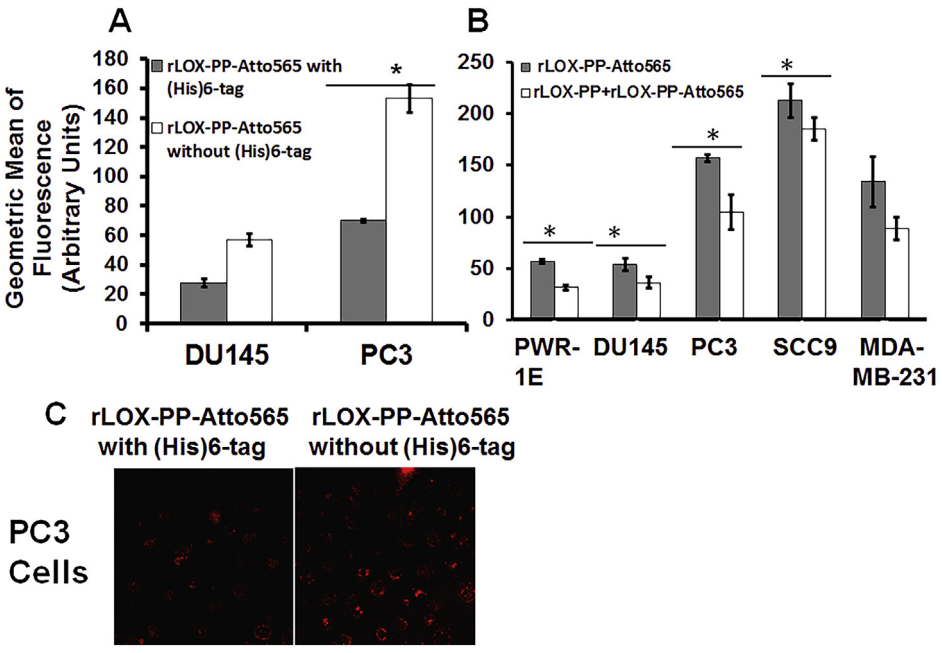

Figure 13 – Removal of $(His)_6$-tag increases rLOX-PP-Atto565 uptake, while pretreatment with rLOX-PP decreases its uptake. In (A), DU145 cells and PC3 cells were treated with either rLOX-PP-Atto565 with His-tag (gray bars) or without $(His)_6$-tag (white bars), and uptake levels quantified as a function of time by flow cytometry; n = 3, *, p < 0.005. (B) Cells were pre-treated with unlabeled rLOX-PP, followed by rLOX-PP-Atto56, and uptake of rLOX-PP-Atto565 determined; data are means ± SD, n = 3, *, two-tailed p < 0.05 (Except in MDA-MB-231). (C) A representative confocal image showed that removal of $(His)_6$-tag increased rLOX-PP-Atto565 uptake in PC3 cells at 3 h (images were collected with EC-Plan Neofluar 40x/1.30 oil DIC M27 objective).

with functional consequences (Bais et al., 2015b; Sanchez-Morgan et al., 2011; Sato et al., 2011, 2013). Moreover, nuclear localization of rLOX-PP has been demonstrated in cell confocal microscopy and cell fractionation studies (Bais et al., 2015b; Guo et al., 2007).

3.2. *Dynamin-dependent uptake of rLOX-PP-Atto565*

3.2.1. *Caveolae mediated uptake for rLOX-PP-Atto565 internalization*

Additional LOX-PP uptake pathways also occurred to varying degrees in other cell lines. Our inhibition experiments by siRNA mediated caveolin-1 knockdown in PWR-1E, PC3, MDA-MB-231 cells suggest that a caveolae-mediated uptake pathway for rLOXPP-Atto565 occurs. The importance of caveola-mediated uptake is that it is a nonacidic and non-digestive route of internalization (Gassner and Komnick, 1983; Wang et al., 2004). The presence of caveolin-1 on early endosomes or caveosomes provides evidence for intracellular trafficking of caveola-mediated uptake. Cargo is delivered from caveolin-1 presenting vesicles to the endoplasmic reticulum and trans Golgi network (Chaudhary et al., 2014; Parton, 2004). rLOX-PP may be delivered to intracellular locations via caveolae-mediated uptake through early endosomes or independent of the endosomal/lysosomal pathway. This appears to occur in the PWR-1E, PC3, MDA-MB-231 cell lines.

Interestingly, caveolin-1 knockdown in SCC9 cells increased rLOXPP-Atto565 uptake, in contrast to effects seen in PC3, and MDA-MB-231 cells. It was previously reported that the constitutive phosphorylation of caveolin-1 in cells functions for intracellular cholesterol trafficking (Li et al., 2013; Torgersen et al., 2001). Caveolin-1 accumulates reversibly at the outer surface of lysosomes in serum depleted cells but not in serum treated cells due to an increase of endosomal pH (Mundy et al., 2012). Knockdown of caveolin-1 stops intracellular cholesterol trafficking. Moreover, caveolae pathway is compensated by the CLIC/GEEC pathway in cells lacking caveolin-1 or in cells with down-regulated expression of caveolin-1 (Chaudhary et al., 2014). We suggest that increased rLOX-PP-Atto565 uptake in caveolin-1 knocked-down SCC9 cells may be independent from caveolae-mediated uptake. The increased intracellular pH mediated by alkalizing effect of rLOX-PP-Atto565 and serum depletion may stimulate PI3K dependent macropinocytosis in SCC9 cells. Knocking-down of caveolin-1 may stimulate the CLIC/GEEC pathway in SCC9 cells and result in increased rLOX-PP-Atto565 uptake without caveolin1 phosphorylation. In addition, rLOX-PP-Atto565 accumulation on the plasma membrane boundary in caveolin-1 knockdown SCC9 cells may indicate that caveolin-1 plays a role on the intracellular distribution of rLOX-PP-Atto565 but not on its uptake in SCC9 cells. Despite the high level of caveolin-1 phosphorylation, rLOX-PP-Atto565 uptake was not significantly reduced in PWR-1E cells by caveolin-1 knockdown (Figures 7A and 8A). It was demonstrated that endogenous LOX-PP level was high in PWR-1E cells (Data not shown). That may reduce the demand for rLOX-PP-Atto565 uptake and may mask the role of caveolae-mediated rLOX-PP-Atto565 in PWR-1E cells.

3.2.2. *Clathrin-mediated uptake for rLOX-PP*

Clathrin-mediated uptake of cargo occurs by formation of clathrin coated pits in response to cell binding and activation of adaptor protein-2 (AP2). Clathrin coated pits are pinched off from the plasma membrane by dynamin (Bonifacino and Lippincott-Schwartz, 2003; Gruenberg and Stenmark, 2004; Kirchhausen, 2000). The clathrin dependent pathway delivers cargo to recycling endosomes or alternatively multi-vesicular bodies for endosomal degradation.

Transferrin binds to the transferrin receptor and directs clathrin coated vesicles by AP2. Therefore, co-localization of rLOX-PP-Atto565 with transferrin provides evidence that rLOX-PP-Atto565 uses the same pathway for uptake. Here we detected a partial co-localization of rLOX-PP-Atto565 with the transferrin-FITC only in PC3 cells (Figure 9). In addition, in PC3 cells a partial decrease of rLOX-PP-Atto565 uptake and the total inhibition of transferrin-FITC uptake in PC3 cells occurred in presence of dynasore, while the macropinocytosis tracker 10 kDa dextran-Bodipy-fl internalization was not affected. Short-term treatment with 100 μM dynasore for 3 h decreased rLOX-PP-Atto565 uptake in only PC3 cells. Data indicate that while the major rLOX-PP-Atto565 uptake pathway in PC3 cells is by macropinocytosis, these cells also employ a dynamin-and clathrin dependent uptake mechanism for rLOX-PP-Atto565 internalization. The knowledge that rLOX-PP-Atto565 can be taken up by cells via different pathways and that these pathways vary may provide opportunities to target cells in a specific environment that utilize a relatively rare uptake pathway.

3.2.3. *Endosomal pH modification caused by rLOX-PP-Atto-565/647N uptake*

Reduced uptake of rLOX-PP-Atto565 by bafilomycin A1 was observed in all cell lines (Figure 11A). It is likely that bafilomycin increased recycling of rLOX-PP-Atto565, resulting in the observed effect. It was reported that bafilomycin A1 at concentrations over 200 nM completely inhibits endosomal membrane acidification and arrests further progression of early endosomes (Bayer et al., 1998). Alkalinization of endosomes thus may promote the recycling of rLOX-PP-Atto565, but may not affect the initial uptake of rLOX-PP-Atto565.

By contrast, EIPA which reduces pH in primary coated vesicles, early endosomes and recycling endosomes also suppresses pH sensitive Rac1 and Cdc42 GTPases required for actin remodeling (Koivusalo et al., 2010). Thus, EIPA treatment inhibits macropinocytosis of macromolecules unless the decreased intracellular pH caused by EIPA treatment is reversed by the cargo itself (Koivusalo et al., 2010; Nowak-Lovato et al., 2010). The basis for increased rLOX-PP-Atto565 uptake in the presence of EIPA could be multifactorial. The first factor may be inhibition of recycling by the reduced alkalinization of recycling endosomes by EIPA treatment. The second factor may be the restoration of Rac1 function for proper macropinosome formation by the alkalinizing effect of internalized basic rLOX-PP-Atto565. The third factor may be the acceleration of rLOX-PP-Atto565 initial uptake by a favorable low pH condition caused by EIPA treatment. rLOX-PP-Atto565 appears to have a tendency to accumulate in low pH macropinosomes during its internalization.

Based on our in situ pH measurement data, we propose that instead of decreasing recycling by EIPA, the resulting low pH caused by EIPA increased rLOX-PP uptake and restored Rac1 functions and PI3K-dependent macropinocytosis. Nuclear localization or evidence of endosomal escape of rLOX-PP in various cell lines were previously reported (Bais et al., 2015a; Guo et al., 2007). In addition, increased rLOX-PP uptake in EIPA treated cells may be correlated with restored Rac1 function via increased endosomal pH by rLOX-PP-Atto565 treatment. The elevation of rLOX-PP charge in low pH conditions may help to drive it into low pH environments. Based on theoretical rLOX-PP charge calculations and on pH values measured in Figure 12 (Joshi et al., 2012), we suggest that after cellular entry, rLOX-PP-Atto647N increases endosomal pH to favorable conditions for its own uptake. Its buffering capacity appears to maintain endosome pH higher than pH 6.84 and inhibits endosomal maturation. Subsequently, rLOX-PP would be arrested in macropinosomes. rLOX-PP could then either escape into the cytoplasm or recycle to the cell surface via an actin-dependent fast recycling pathway. The pH achieved by EIPA treatment after rLOX-PP (pH 6.87) may not be favorable for promoting the recycling of rLOX-PP. However, the pH under EIPA treatment conditions may be sufficient to restore Rac1 function for promoting PI3K-dependent macropinocytosis.

By contrast, the high endosomal pH generated by bafilomycin A1 treatment decreased rLOX-PP uptake possibly by increasing rLOX-PP recycling. Even though bafilomycin A1 treatment alone increased the endosomal pH from 6.77 to 6.95, the endosomal pH increased only to 6.84 in cells treated with rLOX-PP plus bafilomycin A1 (Figure 12B). Thus, we conclude that rLOX-PP decreased the endosomal pH from 6.95 to 6.84 in the presence of bafilomycin A1. Therefore, we proposed that, by increasing endosomal pH from 6.77 to 6.84, rLOX-PP may decrease its own intracellular level by increasing actin-dependent recycling.

The next studies investigated whether the high positive electrostatic charge rLOX-PP-Atto565 at cell entry and at endosomes could promote its interaction with negatively charged plasma membranes or vacuole membranes. Uptake of rLOX-PP-Atto565 without the $(His)_6$-tag was, therefore, evaluated. As noted, labeled rLOX-PP was significantly elevated in both DU145 and PC3 cells at 3 h of endosomal uptake. These findings further support the notion that the cationic charge of rLOX-PP-Atto565 may be responsible for the endosomal alkalization and restoration of its uptake by macropinocytosis in low pH conditions. Altogether, data support that an increased pI value elevated rLOX-PP-Atto565 affinity to low pH of endosomes and increased the uptake of rLOX-PP-Atto565.

4. Conclusions

In summary, the major uptake pathway for labeled rLOX-PP appears to be primarily PI3K-dependent macropinocytosis. Secondary pathways appeared to be dynamin- and caveola dependent for labeled rLOX-PP uptake by PWR-E1, PC3, MDA-MB-231 cell lines (Table 1). Both macropinocytosis- and caveola dependent uptake pathways are favorable for escape from endosomes to the cytoplasm and escape from lysosomal

Table 1 – Summary of Pathways for rLOX-PP Uptake.

Cell Line	Minor pathways		Major pathways	
	Dynamin-dependent uptake		Dynamin-independent macropinocytosis	
	Clathrin (Dynasore)	Caveolae (Caveolin-1 siRNA)	Actin (Cytochalasin D)	PI3K (LY294002)
PWR-1E		+	+	+
DU145			+++	
PC3	+	+++	+	++
SCC9			++	+
MDA-MB-231		+++	++	+

The symbols +++, ++, and + respectively indicate high-, intermediate-, or low involvement of the respective pathway. Parentheses identify the inhibitor of the pathway which provides evidence for the indicated outcome.

degradation (Cain et al., 1989; Clerc and Sansonetti, 1987; Garcia-del Portillo and Finlay, 1994; Goosney et al., 1999; Harris et al., 2002; Khalil et al., 2006; Zenni et al., 2000). It appeared that the elevation of the cationic charge of labeled rLOX-PP may help to drive labeled rLOX-PP into low pH environments. Furthermore, the endosomal alkalinizing effect of rLOX-PP demonstrated may restore Rac1 or PI3K dependent macropinocytosis in cells with a low intracellular pH. This property may increase the uptake of rLOX-PP in tumors compared to normal tissues in vivo. This notion is based on the excess production of lactic acid under hypoxic conditions in tumors resulting in relatively low pH(i) (Tannock and Rotin, 1989). The proposed model for rLOX-PP uptake and subsequent mechanisms and effects of drug treatments are summarized in Figure 14.

5. Materials and methods

5.1. Cells and reagents

PWR-1E, DU145, PC3, SCC9, and MDA-MB-231 cell lines were obtained from the American Type Culture Collection (Manassas, VA, USA). Head-and-neck squamous cell carcinoma UMSCC2 was a gift kindly provided by Dr. Roberto Weigert of NIH/NIDCR. Cells were not used after passage 10. QSY® 9 carboxylic acid succinimidyl ester was purchased from Molecular Probes, Eugene, OR (#Q20131). Transferrin-FITC, 10 kDa dextran-Bodipy conjugate, recombinant cholera toxin subunit B Alexa Fluor® 647 conjugate (#C34778), Hoechst 33342 nuclear dye, Phalloidin-Alexa488, α2-(4-pyridyl)-5-[(4-(2–dimethyl-

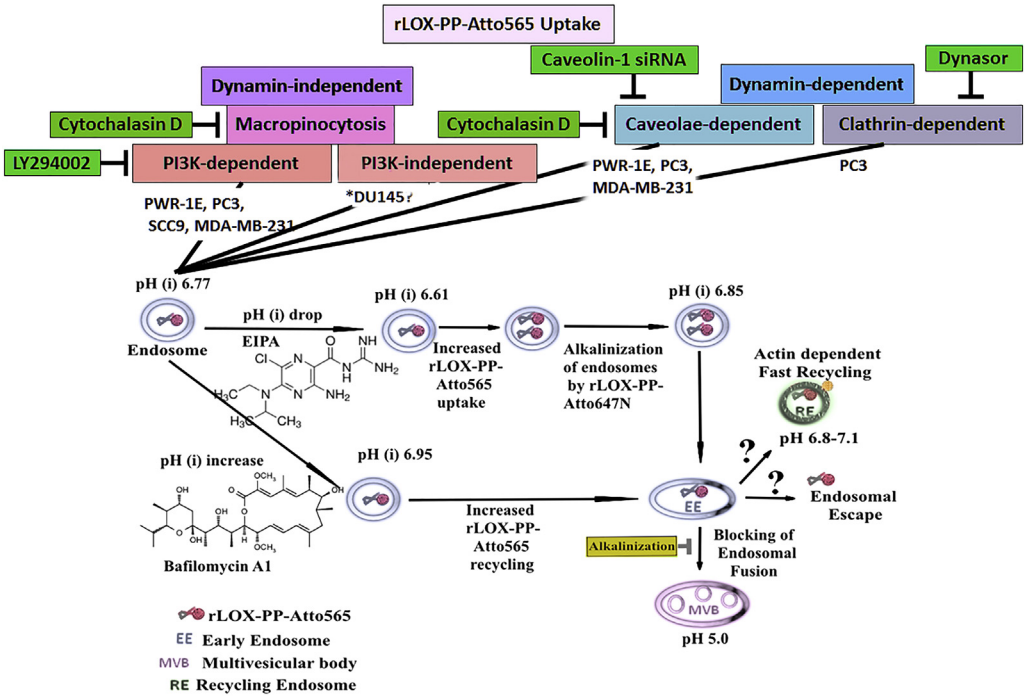

Figure 14 – Schematic representation of different intracellular uptake pathways of rLOX-PP-Atto565. Postulated mechanisms of rLOX-PP-Atto565 uptake are shown and the cell lines which use a particular uptake mechanism are indicated. They include actin- and PI3K-dependent macropinocytosis, dynamin-clathrin-dependent endocytosis and dynamin-caveolae-dependent endocytosis. The effect of pH change by EIPA, bafilomycin A1 and rLOX-PP itself on subsequent rLOX-PP-Atto647N trafficking was shown. *rLOX-PP-Atto565 uptake in DU145 cell is not PI3K-dependent macropinocytosis.

amino-ethyl-amino-carbamoyl) methoxy)-phenyl] oxazole (PDMPO) fluorescent dye Lysosensor Yellow/Blue dextran 10,000 MW (#L22460), 5-(N-ethyl-N-isopropyl) amiloride, hydrochloride (EIPA-#E3111), and SYTO® 11 Green Fluorescent Nucleic Acid Stain (#S7573), Lipofectamine® 2000 Transfection Reagent (#11668019) all were purchased from Life Technologies (Grand Island, NY). ECL Plex Fluorescent Rainbow Markers IMPROVED (120ul) (#RPN850E) was purchased from GE Healthcare. AKT antibodies were purchased from Cell Signaling (#9272 and #9275), SMARTpool: ON-TARGETplus CAV1 siRNA and negative control siRNA were purchased from Dharmacon. All other reagents were purchased from Sigma/Aldrich, Antibodies-online.com (caveolin-1 antibodies) or Thermo Fisher Scientific and were of the highest quality available. rLOX-PP was expressed in human TREX-293 cells and purified as described (Vora et al., 2010a).

5.2. *In vivo analysis of LOX-PP activity against oral cancer*

UMSCC2 cells expressing DsRed to permit IVIS imaging were generated as previously described (Bais et al., 2015a). rLOX-PP expressing lentivirus and empty lentivirus previously generated and employed (Bais et al., 2015b) were then respectively used to transduce DsRed-UMSCC2 cells to generate two new lines UMSCC2 expressing DsRED plusLOX-PP, and control transduced cells expressing only DsRed. These cells (0.5×10^6 cells in 40 μl) were respectively injected into the tongues of two month old nude mice (NCr nu/nu, n = 9/ group; Taconic Farms, Hudson, NY), in respective groups after anesthetizing with 4% isoflurane. Caliper measurements were performed at regular intervals to monitor the volumes of all tumors. Mice were imaged at intervals for DsRed protein expression using an IVIS 200 system (Xenogen, Alameda, CA, USA). Anesthesia was administered in an induction chamber with 2.5% isoflurane in 100% oxygen at a flow rate of 1 L/min and then maintained with a 1.5% mixture at 0.5 L/min. The fluorescence signals were optimized for DsRed protein at excitation 570 nm and emission 620 nm. Fluorescence region of interest (ROI) data are then calibrated, normalized fluorescence efficiency $(p/sec/cm^2/sr)/(\mu W/cm^2)$ as per the instructions (Perkin Elmer, USA). The data are reported as normalized fluorescence intensity (FU) from a defined region of interest for oral tongue tumors or systemic metastases compared to control vehicle-injected mice.

5.3. *rLOX-PP labeling with Atto565*

rLOX-PP was labeled at the N-terminus and at the only lysine residue which is located in the C-terminal myc-$(His)_6$-tag employing the N-hydrosuccinamide (NHS) ester of Atto-565(4-[4-(dimethyl-amino)-phenylazo]-benzoic acid) (Molecular Probes, Eugene, OR). LOX-PP itself has no lysine residues or cysteine residues which would become modified under these conditions (Vora et al., 2010a).

rLOX-PP (2 mg/ml) in 0.1 M sodium bicarbonate buffer (pH 8.3) was mixed with a 10-fold molar excess of Atto-565-NHS ester and incubated at 37 °C for 3 h, followed by incubation at 4 °C overnight (Nakano et al., 2012; Wang et al., 2008). The samples were adjusted to a final urea concentration of 4 M and subjected to Sephadex G-25 gel filtration chromatography (GE Healthcare, Waukesha, WA, PD MiniTrap™ G-25, #28-9180-07) pre-equilibrated in 200 mM sodium phosphate buffer with 10 M urea (pH 7.8) and eluted with same buffer at room temperature. The flow-through fraction containing Atto565 labeled rLOX-PP (rLOX-PP–Atto565) was collected. rLOX-PP–Atto565 was then dialyzed against water to remove urea using 10,000 Dalton molecular weight cut off Slide-A-Lyzer dialysis cassettes at 4 °C overnight (Thermo Scientific, Waltham, MA) and an aliquot subjected analytical 12% SDS PAGE gel and imaged (Ex 565 nm, Em 592 nm) with a Molecular Imager Pharos-FX (Bio-Rad) to confirm free dye removal (Figure S5A) (Biorad, Hercules, CA). The stoichiometry of Atto565 labeling efficiency was calculated based on extinction coefficients of rLOX-PP and Atto-565. The extinction coefficient of Atto-565 is 120,000 L mol^{-1} cm^{-1} at 563 nm and rLOX-PP is 19,480 L mol^{-1} cm^1 at 280 nm rLOX-PPAtto565 stocks were stored in aliquots at −20 °C.

5.4. *rLOX-PP-Atto565 uptake for confocal microscopy*

Uptake studies were performed in live cells by plating 30,000 cells in 4-well Nunc® Lab-Tek® II Chamber Slides™ in DMEM containing 10% FBS, 1% penicillin-streptomycin and cultured overnight. The cells were replenished with media containing 0.1% BSA, 1% penicillin-streptomycin for 12 h rLOX-PP-Atto565 was then added in the presence or absence of uptake inhibitors and incubated as a function of time. The cells were imaged with a Zeiss Axiovert 100M inverted fluorescence microscope or a Zeiss 710 dual scanner confocal microscope as indicated. As a negative control, cell impermeable chicken egg white lysozyme (Sigma–Aldrich #L7001) was labeled and purified and concentration calculated with same protocol used for rLOX-PP labeling, and was found not to enter cells.

5.4.1. *Quenching of both extracellular fluorescence and fluorescence from dead cells*

A Förster resonance energy transfer (FRET) quencher was generated from N-ε-(carboxymethyl)-lysine-bovine serum albumin (CML-BSA) (Khosravi et al., 2014) labeled with QSY® 9 Carboxylic Acid, Succinimidyl Ester (CML-BSA-QSY9) to quench extracellular Atto565 fluorescence in live cells and in both dead and membrane permeable cells. Fluorescence emission was collected by using Tristar LB 941 plate reader at 592 nm. From a modified Stern-Volmer plot (Banerjee and Rao, 2011) it was determined that an 80 times higher concentration of CML-BSA-QSY9 quenched 95% of Atto565 fluorescence of rLOX-PP-Atto565 and chicken egg white lysozyme-Atto565 independent of cell size in all cell lines tested (data is not shown). To test efficacy of quenching method, DU145 and PC3 cells were next treated with 0.2 μM rLOX-PP-Atto565 or 0.2 μM chicken egg white lysozyme-Atto565 for 3 h washed with PBS for 3 times and treated with 16 μM CML-BSA-QSY9 for 15 min at 4 °C and replenished media with PBS and imaged using Zeiss Axiovert 100M inverted fluorescence microscope (Figure S5B–C). Therefore, the concentration of CML-BSA-QSY9 which quenched extracellular fluorescence of cell impermeable 0.2 μM chicken egg white lysozyme-Atto565 fluorescence was experimentally determined. Atto565 fluorescence from plasma membrane permeable and dead cells or

cell surface fluorescence from live cells was subsequently quenched by treatment with CML-BSA-QSY9 under these conditions before both confocal microscopy and flow cytometry. The quenching procedure in both confocal microscopy and flow cytometry experiments was done for 15 min at 4 °C to avoid endocytosis of CML-BSA-QSY9 quencher. In addition, to avoid stimulation of caveolae-dependent uptake pathway unconjugated QSY9 quencher dye was used in both confocal and flow cytometry experiments related to caveolae-dependent uptake of rLOX-PP-Atto565. To quench cell surface fluorescence in live cells and intracellular fluorescence in membrane permeable and dead cells from rLOX-PP-Atto565 and CtxB-Alexa647 fluorescence, 3 μM QSY9 dye was used in both confocal and flow cytometry experiments. (Figures 5–6A).

5.4.2. *rLOX-PP double labeling with Atto565 and QSY9*

To determine optimum time points for analysis of intact rLOX-PP uptake, we determined the stability of rLOX-PP as a function of time. For this purpose, we generated double-labeled rLOX-PP by sequential labeling rLOX-PP with Atto565 followed by a quencher tag QSY9 resulting in a non-fluorescent intact rLOX-PP that would become fluorescent after hydrolysis resulting from separation of the quencher and Atto565.

5.4.3. *Western blot degradation assay*

We independently analyzed the degradation level of rLOX-PP-Atto565 in DU145 and PC3 cell lysates by probing Western blots with LOX-PP antibody and calculated levels of degraded and intact rLOX-PP-Atto565 in cell layers and media. Band fluorescence levels were analyzed with a Molecular Imager Pharos-FX (Bio-Rad) imager and quantified with image J (Figure S2).

5.4.4. *Confocal laser scanning microscopy for live cell imaging*

Confocal laser scanning microscopy was performed on Zeiss LSM 710 dual scanner confocal microscope equipped with Plan-Apochromat 100x/1.46 Oil DIC at objective and ZEN 2011 software (Carl Zeiss, Gottingen, Germany). For some experiments Zeiss Axiovert 100M inverted fluorescence microscope was used. All co-localization studies were performed with living, non-fixed cells grown in Nunc® Lab-Tek® II Chamber Slide™ system, 4 well chamber slides. Cells were seeded at a density of 30,000/well 12 h before the experiment and cultured in media supplemented with 10% fetal bovine serum and 1% penicillin-streptomycin. The cells were replenished with media containing 0.1% BSA, 1% penicillin-streptomycin for 12 h 0.1% BSA was not used in the caveolae-related experiments so as not to independently activate CAV-1. rLOX-PP-Atto565 and a tracker were added and incubated for 3 h. All quantification and co-localization studies were done with live cells to avoid the efflux of rLOX-PP-Atto565 from cells and artifactual co-localization of rLOX-PP-Atto565 with the uptake trackers throughout microscopy experiments. Before imaging the cell surface was quenched with CML-BSA-QSY9 in live cells and intracellular fluorescence was quenched with CML-BSA-QSY9 in dead cells and membrane permeable cells to exclude detection of cell surface or damaged cell-bound rLOX-PP-Atto565 in the confocal microscope images. Live cells were stained for nuclei with 2.0 μg/ml Hoechst 33342 (385/470) dye for 15 min, quenched with CML-BSA-QSY9 for 3 min, maintained in a live cell chamber at 37 °C, 5% CO_2 and imaging including z-stacked images were obtained. Hoechst 33342 (385/470), transferrin-FITC (490/525 nm) and 10 kDa dextran-Bodipy-fl (503/512 nm) and Atto565 (563/592 nm) were exited with a 405 nm diode laser, with a 488 nm multiline argon laser, and with a 561 nm diode pumped solid state laser, consecutively. Active detection channels and photomultiplier (pmt) channels were compensated to avoid fluorescence bleeding over on the other fluorescent dye. Images were evaluated with LSM-viewer and image J software. Merged images were generated by Image J and Photomatix software.

5.4.5. *Immunofluorescence for actin and caveolin-1*

Cells were pretreated with 1.5 μM cytochalasin D or with 100 μM LY294002 for 30 min in Nunc™ Lab-Tek™ II Chamber Slide™ 4 Well System. rLOX-PP-Atto565 (4–10 μg/ml) was then added in presence or absence of cytochalasin D or LY294002 for 15 min on ice and then 30 min at 37 °C, 5% CO_2. The cells were fixed for 10 min at room temperature in a solution containing fixation buffer (137 mM NaCl, 5 mM KCl, 1.1 mM NaH_2PO_4, 0.4 mM KH_2PO_4, 2 mM $MgCl_2$, 2 mM K-EGTA, pH 6.8, and 5.5 mM glucose in 4% paraformaldehyde). Cells were made permeable at −20 °C with 100% methanol for 10 min, and then stained with 25 μg/ml Alexa 488-labeled phalloidin for 30 min. To preserve membrane bound rLOX-PP-Atto565 in Figure 5B1–2 and 3E, fixation buffer and methanol were gently added or removed from same corner of Nunc™ Lab-Tek™ II Chamber Slide™ 4 Well System via pipetting without quenching membrane bound rLOX-PP. For total and phospho-CAV-1 staining, cells were incubated with primary antibodies at 4 °C for overnight and then treated with secondary antibodies labeled with Alexa 647. Before imaging cell nuclei were stained with 2.0 μg/ml Hoechst 33342 in PBS for 30 min, and samples covered with ProLong® Gold antifade reagent to suppress photo-bleaching. Finally, cells were mounted and confocal fluorescence images were recorded using a Zeiss LSM 710 confocal microscope equipped with Plan-Apochromat 100x/1.46 Oil DIC objective and ZEN 2011 software. Images were evaluated with LSM-viewer and image J software. Merged images were generated by Image J and Photomatix software.

5.5. *Quantification of rLOX-PP uptake by flow cytometry*

Cell lines were plated at 0.16×10^6 cells per well (80% confluence) in 24 well plates and maintained at 37°, 5% CO_2 in respective required serum-free media supplemented with 0.1% BSA (except caveolae-related experiments) and 1% penicillin/streptomycin. Cells were then pretreated with predefined uptake inhibitors for 10 min on ice, followed by 30 min at 37 °C, 5% CO_2. Cells were refed with 4 μg/ml (0.2 nM) rLOX-PP-Atto565 in the presence or absence of an uptake inhibitor or vehicle in media supplemented with 0.1% BSA for 3 h. After removal of media, rLOX-PP-Atto565 was washed out with ice cold PBS for 3 times and trypsinized with 25% trypsin for 5 min to detach cells from 24 well-plates and to remove surface bound rLOX-PP-Atto565. Trypsin was

removed by centrifuging cells at 1500 rpm at 4 °C for 5 min. To gate out cell surface bound rLOX-PP-Atto565 fluorescence and intracellular rLOX-PP-Atto565 fluorescence from both dead and plasma membrane permeable cells, cells were treated with a CML-BSA bound dark quencher (CML-BSA-QSY9 at an 80-fold excess over Atto565 dye) on ice for 10 min with gentle agitation, and then centrifuged at 1500 rpm at 4 °C for 5 min to remove CML-BSA-QSY9. In flow cytometry dead cells, doublets, cell residues and background fluorescence from the cells were gated out based on forward scatter (FSC) and side scatter (SCC) parameters to ensure accuracy in all quantification experiments. To calculate the percentage of dead cells in each inhibitor experiment to simultaneously measure toxicity, cells were treated with LIVE/DEAD® Fixable Near-IR stain (Molecular Probes) according to the company's protocol on ice with gentle agitation for 30 min, and then cells were washed three times by centrifugation three times at 1500 rpm at 4 °C for 5 min each. The LIVE/DEAD® Fixable Near-IR stain was employed to determine the percentage of membrane permeable and dead cells in the total population while CML-BSA-QSY9 (or free QSY9 in caveola related experiments only) was used to quench Atto565 fluorescence from cell surfaces, membrane permeable and dead cells. The number of CML-BSA-QSY9 or QSY9 treated membrane permeable and dead cells in the whole population were simultaneously countable with LIVE/DEAD® Fixable Near-IR stain because QSY9 excitation and LIVE/DEAD® Fixable Near-IR emission spectrum did not overlap. Cell suspensions were filtered through a 40 μm nylon mesh filter (Fisher Scientific) and subjected to flow cytometry using a LSR-II flow cytometer (BD Biosciences) with an SSC and FSC detector to exclude debris and cell doublets. To measure fluorescence levels for rLOX-PP-Atto565, Atto565 was excited with yellow/green laser (561 nm) and emission was counted using a pre-set PE-Texas Red emission filter (600 LP-610-/20 filter set). LIVE/DEAD® Fixable Near-IR dye was exited with a red laser (633 nm) and fluorescence emission was collected pre-set infrared emission filter APC-CY7 (735LP-760/60 emission filter set) to exclude dead cells. All flow cytometry experiments were performed in triplicate at least three separate times and each time 5000 cells were quantified.

5.6. *siRNA-mediated knockdown of caveolin-1 expression*

Cells were grown in six-well plates. They were transfected by lipofectamine 2000 transfection reagent with 50 nM ON-TARGETplus human CAV-1 SMART pool siRNA. Target sequences CUAAACACCUCAACGAUGA, GCAAAUACGUAGACUCGGA, GCAGUUGUACCAUGCAUUA, and GCAUCAACUU GCAGAAAGA; or with 50 nM ON-TARGETplus non-targeting pool siRNA. Immunoblotting analysis or microscopy studies were performed 72 h post-transfection.

5.7. *Endosome pH measurements*

SCC9 cells were selected because they efficiently take up rLOX-PP which appears to occur exclusively by macropinocytosis. Cells were seeded at 0.14×10^6 cells/well or 80% visual confluence into Nunc™ Lab-Tek™ II Chamber Slide™ 4 Well Systems for 24 h in a 1:1 mixture of Dulbecco's modified Eagle's medium and Ham's F12 medium containing 15 mM HEPES supplemented with %10 FBS.

The extracellular pH of tumor cells is acidic and varies from cell to cell based on endogenous metabolism. The low flux rate relative to proton production rates generates acidic steady-state pH gradients in tumor cells (Schornack and Gillies, 2003). Therefore, to determine the endosomal pH accurately the steady-state extracellular pH of SCC9 was first identified under the required experimental conditions in order to establish the working pH for the extracellular solution (*i.e.*, recording buffer) during endosomal pH measurements. The objective here is to match the pH of the extracellular solution to the steady state extracellular pH of SCC9 cells. To define this pH, SCC9 cells were treated with a recording buffer for 3, 6, 12 or 24 h at 37 °C. The recording buffer employed was a bicarbonate (HCO_3)-free buffer with140 mM NaCl, 5 mM KCl, 1 mM MgCl2, l mM CaCl2, 10 mM glucose, 20 mM HEPES with NaOH at pH 7.4 (Barriere et al., 2009). At each time point, extracellular pH was recorded precisely with a pH electrode (at 37 °C) to control for temperature effects on pH to two decimals. After 12 h, the pH had dropped from 7.4 to 7.15 and remained at a steady-state. Thus, the recording buffer pH for experiments was established as pH 7.15 for the remaining experimental conditions because measurement of endosomal pH occurred at 12 h after seeding cells into Nunc™ Lab-Tek™ II Chamber Slide™ 4 Well Systems.

Next, to determine the basal endosomal pH, SCC9 cells were loaded with Lysosensor Yellow/Blue dextran 10,000 MW at pH 7.15 by incubating with 2 μM Lysosensor Yellow/Blue dextran 10,000 MW 3 h prior to the pH measurement in recording buffer. 10 kDa dextran labeled with Lysosensor Yellow/Blue DND-160 fluorescent dye was used to track fluid-phase uptake and to measure endosomal pH, as described (Barriere et al., 2009; Han and Burgess, 2010; Lin et al., 2003; Nixon et al., 2012) and as follows. To establish a calibration curve, bicarbonate (HCO_3)-free MES and HEPES calibration buffers were prepared with 140 mM KCl, l mM MgCl2, 0.2 mM EGTA, 20 mM HEPES (pH between 7.0 and 8.5) or with MES (pH between 4.5 and 6.5) and was adjusted with KOH or HCl in dH2O supplemented with 5 μg/ml monensin and 5 μg/ml nigericin to render cells permeable and to equilibrate endosomal pH to the extracellular pH. After replacing recording buffer with calibration buffers at a variety of pH values, live cell images for the calibration curve were immediately acquired and recorded using a Zeiss LSM 710 confocal microscope equipped with Plan-Apochromat 40x/1.3 Oil DIC and ZEN 2011 software. At the same time, live cell images of SCC9 cells cultured in the pH 7.15 recording buffer were obtained. The excitation wavelength was tuned to 730 nm (two photon laser with equal to 365/19 nm excitation wavelength of UV laser), and emission was detected in 3 channels: 470/20, 490/10 and 525/25 nm for Lysosensor Yellow/Blue dextran 10,000 MW. Lysosensor Yellow/Blue dextran 10,000 MW loaded macropinosomes were identified as those vesicles with diameters between 0.2 and 5 μm to exclude late endosomes, lysosomes and other vacuolar organelles (Wang et al., 2014).

After identification of those macropinosomes, single wavelength fluorescence images obtained at 470/20, 490/10 and 525/25 nm emissions with the same detector and laser setup

were used to calculate the fluorescent intensity ratio of 470/20 nm to 525/25 by Image J according to the protocol (Wang et al., 2014). The isobestic point of Lysosensor Yellow/Blue dextran 10,000 MW at 490/10 nm from each set of images were used as the check point for loading concentration. Therefore, endosomal basal pH of SCC9 cells in recording buffer was by comparing the fluorescent intensity ratio of 470/20 nm to 525/25 nm to pH calibration curve, resulting in the endosomal pH determination of pH 6.77 using the pH calibration curve (Figure S4). Endosomal pH measurements were similarly measured in the presence of rLOX-PP, bafilomycin A1, EIPA or rLOX-PP combined with bafilomycin A1or EIPA to observe endosomal pH changes and buffering capacity of rLOX-PP in recording buffer at pH 7.15. In these experiments, rLOX-PP labeled with pH insensitive Atto647N fluorescent dye to select endosomes loaded with rLOX-PP for the endosomal pH measurements and to avoid fluorescent bleeding over Lysosensor Yellow/Blue dextran 10,000 MW channels. rLOX-PP-Atto647N fluorescent emission was collected at 669/25 nm.

For these experiments, cells were initially pre-treated with bafilomycin A1 or EIPA or vehicle for 30 min in recording buffer. Then, cells were loaded with 2 μM Lysosensor Yellow/Blue dextran 10,000 MW for 3 h in the presence or absence of 0.2 μM rLOX-PP-Atto647N in the recording buffer at pH 7.15 with bafilomycin A1 or EIPA or vehicle and then imaged.

Fluorescence intensity of punctate images or endosomes between 0.2 and 5 μm size was analyzed using Image J and the fluorescence intensity ratio of 470 nm–525 nm was calculated. For each sample, the fluorescent intensity of at least 20 spots were analyzed from each of three replicate wells per sample. Standard curves of pH vs. fluorescence ratio between 470 nm and 525 nm were plotted, and a polynomial equation was generated as a reference for pH measurement in SCC9 cells. Images of both channels (470 nm and 525 nm) were imported into Image J and image calculator was used to divide the images from channel 470 nm by images from channel 525 nm, and a new set of images was saved as a pH profile.

5.8. *Removal of $(His)_6$-tag residues from rLOX-PP-Atto565*

39.5 μM rLOX-PP-Atto565 was mixed with carboxypeptidase A (50 IU/ml) in pH 7.6 buffer (25 mM Tris-HCL, 14. mM beta-mercaptoethanol, 500 mM NaCl) and incubated for 6 h at room temperature followed by 24 h at 4 °C in a final volume of 200 μl, and (His)6-free LOX-PP purified by Heparin Sepharose chromatography in PBS, washed with PBS, and hydrolyzed rLOX-PP-Atto565 eluted with 8 M urea in 0.2 M sodium phosphate buffer pH 7.8. The recovered LOX-PP-Atto565 without $(His)_6$-tag residues was further purified on a G-25 column in 8 M urea buffer (pH 7.8). Finally, 1 mM EDTA added in the elution to neutralize any carboxypeptidase A remnant. The eluate was then dialyzed in 10 kDa cut-off cassette against dH2O for 2 times, 1 h each once overnight. Based on both rLOX-PP and Atto565 extinction coefficients the labeling efficiency was unchanged as expected. Purity of rLOX-PP-Atto565 without the $(His)_6$ tag was verified by 12% SDS-PAGE and a Western blot was probed with rLOX-PP antibody (Hurtado et al., 2008) and anti $(His)_6$ antibody (data not shown).

5.9. *Western blot inhibition assay for FGF2 mediated AKT phosphorylation with both Atto565 labeled and non-labeled rLOX-PP*

To compare the functionality of labeled and non-labeled rLOX-PP, FGF2-stimulated AKT phosphorylation inhibition assay was carried out with both labeled and non-labeled rLOX-PP (0.2 μM). Serum starved cells were treated with either rLOX-PP or rLOX-PP-Atto565 for 24 h and then AKT phosphorylation was stimulated with FGF-2 (10 ng/ml) for 10 min. Cell lysates were collected and subjected to SDS-PAGE and Western blotting using total and phospho-specific antibodies against AKT (Figure S1).

6. Statistical analysis

Analyses of all experiments were done using Student's *t*-test as indicated in Figure legends. All experiments were performed at least three times. Values of $p < 0.05$ were accepted as significant.

Conflict of interest statement

All authors declare that they have no conflicts of interest regarding the contents of this manuscript.

Acknowledgments

This work was supported by NIH grants R21DE023973 and DOD W81XWH-08-1-0349 PC073646.

Appendix A. Supplementary data

Supplementary data related to this article can be found at http://dx.doi.org/10.1016/j.molonc.2015.07.005.

REFERENCES

Ahn, S.G., Dong, S.M., Oshima, A., Kim, W.H., Lee, H.M., Lee, S.A., Kwon, S.H., Lee, J.H., Lee, J.M., Jeong, J., Lee, H.D., Green, J.E., 2013. LOXL2 expression is associated with invasiveness and negatively influences survival in breast cancer patients. Breast Cancer Res. Treat. 141, 89–99.

Amyere, M., Payrastre, B., Krause, U., Van Der Smissen, P., Veithen, A., Courtoy, P.J., 2000. Constitutive macropinocytosis in oncogene-transformed fibroblasts depends on sequential permanent activation of phosphoinositide 3-kinase and phospholipase C. Mol. Biol. Cell 11, 3453–3467.

Araki, N., Hamasaki, M., Egami, Y., Hatae, T., 2006. Effect of 3-methyladenine on the fusion process of macropinosomes in EGF-stimulated A431 cells. Cell Struct. Funct. 31, 145–157.

Araki, N., Hatae, T., Furukawa, A., Swanson, J.A., 2003. Phosphoinositide-3-kinase-independent contractile activities associated with Fcgamma-receptor-mediated phagocytosis

and macropinocytosis in macrophages. J. Cell Sci. 116, 247–257.
Araki, N., Johnson, M.T., Swanson, J.A., 1996. A role for phosphoinositide 3-kinase in the completion of macropinocytosis and phagocytosis by macrophages. J. Cell Biol. 135, 1249–1260.
Bais, M.V., Kukuruzinska, M., Trackman, P.C., 2015a. Orthotopic non-metastatic and metastatic oral cancer mouse models. Oral Oncol. 51, 476–482.
Bais, M.V., Ozdener, G.B., Sonenshein, G.E., Trackman, P.C., 2015b. Effects of tumor-suppressor lysyl oxidase propeptide on prostate cancer xenograft growth and its direct interactions with DNA repair pathways. Oncogene 34, 1928–1937.
Banerjee, A., Rao, D.N., 2011. Functional analysis of an acid adaptive DNA adenine methyltransferase from *Helicobacter pylori* 26695. PloS One 6, e16810.
Bar-Sagi, D., Feramisco, J.R., 1986. Induction of membrane ruffling and fluid-phase pinocytosis in quiescent fibroblasts by ras proteins. Science (New York, N.Y 233, 1061–1068.
Bar-Sagi, D., McCormick, F., Milley, R.J., Feramisco, J.R., 1987. Inhibition of cell surface ruffling and fluid-phase pinocytosis by microinjection of anti-ras antibodies into living cells. J. Cell. Physiol. (Suppl. 5), 69–73.
Barker, H.E., Cox, T.R., Erler, J.T., 2012. The rationale for targeting the LOX family in cancer. Nat. Rev. Cancer 12, 540–552.
Barriere, H., Bagdany, M., Bossard, F., Okiyoneda, T., Wojewodka, G., Gruenert, D., Radzioch, D., Lukacs, G.L., 2009. Revisiting the role of cystic fibrosis transmembrane conductance regulator and counterion permeability in the pH regulation of endocytic organelles. Mol. Biol. Cel. 20, 3125–3141.
Bayer, N., Schober, D., Prchla, E., Murphy, R.F., Blaas, D., Fuchs, R., 1998. Effect of bafilomycin A1 and nocodazole on endocytic transport in HeLa cells: implications for viral uncoating and infection. J. Virol. 72, 9645–9655.
Bonanno, J.A., Giasson, C., 1992. Intracellular pH regulation in fresh and cultured bovine corneal endothelium. I. Na+/H+ exchange in the absence and presence of HCO3. Invest. Ophthalmol. Vis. Sci. 33, 3058–3067.
Bonifacino, J.S., Lippincott-Schwartz, J., 2003. Coat proteins: shaping membrane transport. Nat. Rev. Mol. Cel. Biol. 4, 409–414.
Brabec, M., Schober, D., Wagner, E., Bayer, N., Murphy, R.F., Blaas, D., Fuchs, R., 2005. Opening of size-selective pores in endosomes during human rhinovirus serotype 2 in vivo uncoating monitored by single-organelle flow analysis. J. Virol. 79, 1008–1016.
Cain, C.C., Sipe, D.M., Murphy, R.F., 1989. Regulation of endocytic pH by the Na+,K+-ATPase in living cells. Proc. Natl. Acad. Sci. U.S.A. 86, 544–548.
Chaudhary, N., Gomez, G.A., Howes, M.T., Lo, H.P., McMahon, K.A., Rae, J.A., Schieber, N.L., Hill, M.M., Gaus, K., Yap, A.S., Parton, R.G., 2014. Endocytic crosstalk: cavins, caveolins, and caveolae regulate clathrin-independent endocytosis. PLoS Biol. 12, e1001832.
Clerc, P., Sansonetti, P.J., 1987. Entry of *Shigella flexneri* into HeLa cells: evidence for directed phagocytosis involving actin polymerization and myosin accumulation. Infect. Immun. 55, 2681–2688.
Commisso, C., Davidson, S.M., Soydaner-Azeloglu, R.G., Parker, S.J., Kamphorst, J.J., Hackett, S., Grabocka, E., Nofal, M., Drebin, J.A., Thompson, C.B., Rabinowitz, J.D., Metallo, C.M., Vander Heiden, M.G., Bar-Sagi, D., 2013. Macropinocytosis of protein is an amino acid supply route in Ras-transformed cells. Nature 497, 633–637.
Conner, S.D., Schmid, S.L., 2003. Regulated portals of entry into the cell. Nature 422, 37–44.
Contente, S., Kenyon, K., Rimoldi, D., Friedman, R.M., 1990. Expression of gene rrg is associated with reversion of NIH 3T3 transformed by LTR-c-H-ras. Science 249, 796–798.
Damke, H., Baba, T., van der Bliek, A.M., Schmid, S.L., 1995. Clathrin-independent pinocytosis is induced in cells overexpressing a temperature-sensitive mutant of dynamin. J. Cell Biol. 131, 69–80.
DePedro, H.M., Urayama, P., 2009. Using LysoSensor Yellow/Blue DND-160 to sense acidic pH under high hydrostatic pressures. Anal. Biochem. 384, 359–361.
Drose, S., Altendorf, K., 1997. Bafilomycins and concanamycins as inhibitors of V-ATPases and P-ATPases. J. Exp. Biol. 200, 1–8.
Ellerbroek, S.M., Wennerberg, K., Arthur, W.T., Dunty, J.M., Bowman, D.R., DeMali, K.A., Der, C., Burridge, K., 2004. SGEF, a RhoG guanine nucleotide exchange factor that stimulates macropinocytosis. Mol. Biol. Cel. 15, 3309–3319.
Erler, J.T., Bennewith, K.L., Cox, T.R., Lang, G., Bird, D., Koong, A., Le, Q.T., Giaccia, A.J., 2009. Hypoxia-induced lysyl oxidase is a critical mediator of bone marrow cell recruitment to form the premetastatic niche. Cancer cell 15, 35–44.
Fischer, R., Kohler, K., Fotin-Mleczek, M., Brock, R., 2004. A stepwise dissection of the intracellular fate of cationic cell-penetrating peptides. J. Biol. Chem. 279, 12625–12635.
Foy, R.L., Chitalia, V.C., Panchenko, M.V., Zeng, L., Lopez, D., Lee, J.W., Rana, S.V., Boletta, A., Qian, F., Tsiokas, L., Piontek, K.B., Germino, G.G., Zhou, M.I., Cohen, H.T., 2012. Polycystin-1 regulates the stability and ubiquitination of transcription factor Jade-1. Hum. Mol. Genet. 21, 5456–5471.
Fradet, A., Sorel, H., Depalle, B., Serre, C.M., Farlay, D., Turtoi, A., Bellahcene, A., Follet, H., Castronovo, V., Clezardin, P., Bonnelye, E., 2013. A new murine model of osteoblastic/osteolytic lesions from human androgen-resistant prostate cancer. PloS One 8, e75092.
Fujii, M., Kawai, K., Egami, Y., Araki, N., 2013. Dissecting the roles of Rac1 activation and deactivation in macropinocytosis using microscopic photo-manipulation. Scientific Rep. 3, 2385.
Garcia-del Portillo, F., Finlay, B.B., 1994. Salmonella invasion of nonphagocytic cells induces formation of macropinosomes in the host cell. Infect. Immun. 62, 4641–4645.
Gassner, D., Komnick, H., 1983. Activation and inhibition of Na/K-ATPase by filipin-cholesterol complexation. A correlative biochemical and ultrastructural study on the microsomal and purified enzyme of the avian salt gland. Zeitschrift fur Naturforschung. Section C: Biosci. 38, 640–663.
Gerbal-Chaloin, S., Gondeau, C., Aldrian-Herrada, G., Heitz, F., Gauthier-Rouviere, C., Divita, G., 2007. First step of the cell-penetrating peptide mechanism involves Rac1 GTPase-dependent actin-network remodelling. Biol. cell/under auspices Eur. Cell Biol. Organ. 99, 223–238.
Goosney, D.L., Knoechel, D.G., Finlay, B.B., 1999. Enteropathogenic *E. coli*, *Salmonella*, and *Shigella*: masters of host cell cytoskeletal exploitation. Emerging Infect. Dis. 5, 216–223.
Gruenberg, J., Stenmark, H., 2004. The biogenesis of multivesicular endosomes. Nat. Rev. Mol. Cel. Biol. 5, 317–323.
Guo, Y., Pischon, N., Palamakumbura, A.H., Trackman, P.C., 2007. Intracellular distribution of the lysyl oxidase propeptide in osteoblastic cells. Am. J. Physiol. Cell Physiol. 292, C2095–C2102.
Han, J., Burgess, K., 2010. Fluorescent indicators for intracellular pH. Chem. Rev. 110, 2709–2728.
Harris, J., Werling, D., Hope, J.C., Taylor, G., Howard, C.J., 2002. Caveolae and caveolin in immune cells: distribution and functions. Trends Immunol. 23, 158–164.
Hawkins, P.T., Eguinoa, A., Qiu, R.G., Stokoe, D., Cooke, F.T., Walters, R., Wennstrom, S., Claesson-Welsh, L., Evans, T., Symons, M., et al., 1995. PDGF stimulates an increase in GTP-Rac via activation of phosphoinositide 3-kinase. Curr. Biol. CB 5, 393–403.
Heitz, F., Morris, M.C., Divita, G., 2009. Twenty years of cell-penetrating peptides: from molecular mechanisms to therapeutics. Br. J. Pharmacol. 157, 195–206.

Huang, S.N., Phelps, M.A., Swaan, P.W., 2003. Involvement of endocytic organelles in the subcellular trafficking and localization of riboflavin. J. Pharmacol. Exp. Ther. 306, 681–687.
Hurtado, P.A., Vora, S., Sume, S.S., Yang, D., St Hilaire, C., Guo, Y., Palamakumbura, A.H., Schreiber, B.M., Ravid, K., Trackman, P.C., 2008. Lysyl oxidase propeptide inhibits smooth muscle cell signaling and proliferation. Biochem. Biophysical Res. Commun. 366, 156–161.
Jiang, M., Chen, G., 2009. Ca2+ regulation of dynamin-independent endocytosis in cortical astrocytes. J. Neurosci.: Official J. Soc. Neurosci. 29, 8063–8074.
Jimenez, C., Portela, R.A., Mellado, M., Rodriguez-Frade, J.M., Collard, J., Serrano, A., Martinez, A.C., Avila, J., Carrera, A.C., 2000. Role of the PI3K regulatory subunit in the control of actin organization and cell migration. J. Cell Biol. 151, 249–262.
Joshi, S.N., Butler, D.C., Messer, A., 2012. Fusion to a highly charged proteasomal retargeting sequence increases soluble cytoplasmic expression and efficacy of diverse anti-synuclein intrabodies. mAbs 4, 686–693.
Kaplan, I.M., Wadia, J.S., Dowdy, S.F., 2005. Cationic TAT peptide transduction domain enters cells by macropinocytosis. J. Controlled Release: Official J. Controlled Release Soc. 102, 247–253.
Kato, T., Kawai, K., Egami, Y., Kakehi, Y., Araki, N., 2014. Rac1-dependent lamellipodial motility in prostate cancer PC-3 cells revealed by optogenetic control of Rac1 activity. PloS One 9, e97749.
Kenyon, K., Contente, S., Trackman, P.C., Tang, J., Kagan, H.M., Friedman, R.M., 1991. Lysyl oxidase and rrg messenger RNA. Science 253, 802.
Khalil, I.A., Kogure, K., Akita, H., Harashima, H., 2006. Uptake pathways and subsequent intracellular trafficking in nonviral gene delivery. Pharmacol. Rev. 58, 32–45.
Khosravi, R., Sodek, K.L., Faibish, M., Trackman, P.C., 2014. Collagen advanced glycation inhibits its Discoidin Domain Receptor 2 (DDR2)-mediated induction of lysyl oxidase in osteoblasts. Bone 58, 33–41.
Kirchhausen, T., 2000. Clathrin. Annu. Rev. Biochem. 69, 699–727.
Koivusalo, M., Welch, C., Hayashi, H., Scott, C.C., Kim, M., Alexander, T., Touret, N., Hahn, K.M., Grinstein, S., 2010. Amiloride inhibits macropinocytosis by lowering submembranous pH and preventing Rac1 and Cdc42 signaling. J. Cell Biol. 188, 547–563.
Kozyulina, P.Y., Loskutov, Y.V., Kozyreva, V.K., Rajulapati, A., Ice, R.J., Jones, B.C., Pugacheva, E.N., 2015. Prometastatic NEDD9 regulates individual cell migration via caveolin-1-dependent trafficking of integrins. Mol. Cancer Res. MCR 13, 423–438.
Krzyzaniak, M.A., Zumstein, M.T., Gerez, J.A., Picotti, P., Helenius, A., 2013. Host cell entry of respiratory syncytial virus involves macropinocytosis followed by proteolytic activation of the F protein. PLoS Pathog. 9, e1003309.
Kwong, C., Gilman-Sachs, A., Beaman, K., 2013. An independent endocytic pathway stimulates different monocyte subsets by the a2 N-terminus domain of vacuolar-ATPase. Oncoimmunology 2, e22978.
Levental, K.R., Yu, H., Kass, L., Lakins, J.N., Egeblad, M., Erler, J.T., Fong, S.F., Csiszar, K., Giaccia, A., Weninger, W., Yamauchi, M., Gasser, D.L., Weaver, V.M., 2009. Matrix crosslinking forces tumor progression by enhancing integrin signaling. Cell 139, 891–906.
Li, H.H., Li, J., Wasserloos, K.J., Wallace, C., Sullivan, M.G., Bauer, P.M., Stolz, D.B., Lee, J.S., Watkins, S.C., St Croix, C.M., Pitt, B.R., Zhang, L.M., 2013. Caveolae-dependent and – independent uptake of albumin in cultured rodent pulmonary endothelial cells. PloS One 8, e81903.
Li, M., Morley, P., Tsang, B.K., 1991. Epidermal growth factor elevates intracellular pH in chicken granulosa cells by activating protein kinase C. Endocrinology 129, 2957–2964.
Lin, H.J., Herman, P., Kang, J.S., Lakowicz, J.R., 2001. Fluorescence lifetime characterization of novel low-pH probes. Anal. Biochem. 294, 118–125.
Lin, H.J., Herman, P., Lakowicz, J.R., 2003. Fluorescence lifetime-resolved pH imaging of living cells. Cytometry. Part A: J. Int. Soc. Anal. Cytol. 52, 77–89.
Macia, E., Ehrlich, M., Massol, R., Boucrot, E., Brunner, C., Kirchhausen, T., 2006. Dynasore, a cell-permeable inhibitor of dynamin. Dev. Cell 10, 839–850.
Malyukova, I., Murray, K.F., Zhu, C., Boedeker, E., Kane, A., Patterson, K., Peterson, J.R., Donowitz, M., Kovbasnjuk, O., 2009. Macropinocytosis in Shiga toxin 1 uptake by human intestinal epithelial cells and transcellular transcytosis. Am. J. Physiol. Gastrointest. Liver Physiol. 296, G78–G92.
Mercer, J., Helenius, A., 2008. Vaccinia virus uses macropinocytosis and apoptotic mimicry to enter host cells. Science 320, 531–535.
Mercer, J., Helenius, A., 2009. Virus entry by macropinocytosis. Nat. Cel. Biol. 11, 510–520.
Montesano, R., Roth, J., Robert, A., Orci, L., 1982. Non-coated membrane invaginations are involved in binding and internalization of cholera and tetanus toxins. Nature 296, 651–653.
Moreno-Bueno, G., Salvador, F., Martin, A., Floristan, A., Cuevas, E.P., Santos, V., Montes, A., Morales, S., Castilla, M.A., Rojo-Sebastian, A., Martinez, A., Hardisson, D., Csiszar, K., Portillo, F., Peinado, H., Palacios, J., Cano, A., 2011. Lysyl oxidase-like 2 (LOXL2), a new regulator of cell polarity required for metastatic dissemination of basal-like breast carcinomas. EMBO Mol. Med. 3, 528–544.
Mosesson, Y., Mills, G.B., Yarden, Y., 2008. Derailed endocytosis: an emerging feature of cancer. Nat. Rev. Cancer 8, 835–850.
Mundy, D.I., Li, W.P., Luby-Phelps, K., Anderson, R.G., 2012. Caveolin targeting to late endosome/lysosomal membranes is induced by perturbations of lysosomal pH and cholesterol content. Mol. Biol. Cel. 23, 864–880.
Nakano, D., Kobori, H., Burford, J.L., Gevorgyan, H., Seidel, S., Hitomi, H., Nishiyama, A., Peti-Peterdi, J., 2012. Multiphoton imaging of the glomerular permeability of angiotensinogen. J. Am. Soc. Nephrol. JASN 23, 1847–1856.
Nakase, I., Niwa, M., Takeuchi, T., Sonomura, K., Kawabata, N., Koike, Y., Takehashi, M., Tanaka, S., Ueda, K., Simpson, J.C., Jones, A.T., Sugiura, Y., Futaki, S., 2004. Cellular uptake of arginine-rich peptides: roles for macropinocytosis and actin rearrangement. Mol. Ther. J. Am. Soc. Gene Ther. 10, 1011–1022.
Nakase, I., Tadokoro, A., Kawabata, N., Takeuchi, T., Katoh, H., Hiramoto, K., Negishi, M., Nomizu, M., Sugiura, Y., Futaki, S., 2007. Interaction of arginine-rich peptides with membrane-associated proteoglycans is crucial for induction of actin organization and macropinocytosis. Biochemistry 46, 492–501.
Nixon, R.A., Lee, J.H., Wolfe, D., 2012. Methods for Screening to Identify Therapeutic Agents for Alzheimer's Disease and Use Thereof. Google Patents.
Norbury, C.C., 2006. Drinking a lot is good for dendritic cells. Immunology 117, 443–451.
Nowak-Lovato, K.L., Wilson, B.S., Rector, K.D., 2010. SERS nanosensors that report pH of endocytic compartments during FcepsilonRI transit. Anal. Bioanal. Chem. 398, 2019–2029.
Nylander-Koski, O., Mustonen, H., Puolakkainen, P., Kiviluoto, T., Kivilaakso, E., 2006. Epidermal growth factor enhances

intracellular pH regulation via calcium signaling in acid-exposed primary cultured rabbit gastric epithelial cells. Dig. Dis. Sci. 51, 1322–1330.
O'Connor, K.L., Chen, M., Towers, L.N., 2012. Integrin alpha6beta4 cooperates with LPA signaling to stimulate Rac through AKAP-Lbc-mediated RhoA activation. Am. J. Physiol. Cell Physiol. 302, C605–C614.
Orlandi, P.A., Fishman, P.H., 1998. Filipin-dependent inhibition of cholera toxin: evidence for toxin internalization and activation through caveolae-like domains. J. Cell Biol. 141, 905–915.
Palamakumbura, A.H., Jeay, S., Guo, Y., Pischon, N., Sommer, P., Sonenshein, G.E., Trackman, P.C., 2004. The propeptide domain of lysyl oxidase induces phenotypic reversion of ras-transformed cells. J. Biol. Chem. 279, 40593–40600.
Palamakumbura, A.H., Vora, S.R., Nugent, M.A., Kirsch, K.H., Sonenshein, G.E., Trackman, P.C., 2009. Lysyl oxidase propeptide inhibits prostate cancer cell growth by mechanisms that target FGF-2-cell binding and signaling. Oncogene 28, 3390–3400.
Parton, R.G., 2004. Caveolae meet endosomes: a stable relationship? Dev. Cell 7, 458–460.
Parton, R.G., Joggerst, B., Simons, K., 1994. Regulated internalization of caveolae. J. Cell Biol. 127, 1199–1215.
Paulucci-Holthauzen, A.A., Vergara, L.A., Bellot, L.J., Canton, D., Scott, J.D., O'Connor, K.L., 2009. Spatial distribution of protein kinase A activity during cell migration is mediated by A-kinase anchoring protein AKAP Lbc. J. Biol. Chem. 284, 5956–5967.
Porat-Shliom, N., Kloog, Y., Donaldson, J.G., 2008. A unique platform for H-Ras signaling involving clathrin-independent endocytosis. Mol. Biol. Cell 19, 765–775.
Redelman-Sidi, G., Iyer, G., Solit, D.B., Glickman, M.S., 2013. Oncogenic activation of Pak1-dependent pathway of macropinocytosis determines BCG entry into bladder cancer cells. Cancer Res. 73, 1156–1167.
Reyes-Reyes, E.M., Teng, Y., Bates, P.J., 2010. A new paradigm for aptamer therapeutic AS1411 action: uptake by macropinocytosis and its stimulation by a nucleolin-dependent mechanism. Cancer Res. 70, 8617–8629.
Ridley, A.J., Paterson, H.F., Johnston, C.L., Diekmann, D., Hall, A., 1992. The small GTP-binding protein rac regulates growth factor-induced membrane ruffling. Cell 70, 401–410.
Rinne, J., Albarran, B., Jylhava, J., Ihalainen, T.O., Kankaanpaa, P., Hytonen, V.P., Stayton, P.S., Kulomaa, M.S., Vihinen-Ranta, M., 2007. Internalization of novel non-viral vector TAT-streptavidin into human cells. BMC Biotechnol. 7, 1.
Rossman, J.S., Leser, G.P., Lamb, R.A., 2012. Filamentous influenza virus enters cells via macropinocytosis. J. Virol. 86, 10950–10960.
Rostaing, L., Sanchez-Fructuoso, A., Franco, A., Glyda, M., Kuypers, D.R., Jaray, J., 2012. Conversion to tacrolimus once-daily from ciclosporin in stable kidney transplant recipients: a multicenter study. Transpl. Int. Official J. Eur. Soc. Organ Transplant. 25, 391–400.
Rothenberg, P., Glaser, L., Schlesinger, P., Cassel, D., 1983. Activation of Na+/H+ exchange by epidermal growth factor elevates intracellular pH in A431 cells. J. Biol. Chem. 258, 12644–12653.
Royal, I., Lamarche-Vane, N., Lamorte, L., Kaibuchi, K., Park, M., 2000. Activation of cdc42, rac, PAK, and rho-kinase in response to hepatocyte growth factor differentially regulates epithelial cell colony spreading and dissociation. Mol. Biol. Cell 11, 1709–1725.
Sachdev, P., Zeng, L., Wang, L.H., 2002. Distinct role of phosphatidylinositol 3-kinase and Rho family GTPases in Vav3-induced cell transformation, cell motility, and morphological changes. J. Biol. Chem. 277, 17638–17648.
Sanchez-Morgan, N., Kirsch, K.H., Trackman, P.C., Sonenshein, G.E., 2011. The lysyl oxidase propeptide interacts with the receptor-type protein tyrosine phosphatase kappa and inhibits beta-catenin transcriptional activity in lung cancer cells. Mol. Cell Biol. 31, 3286–3297.
Sandgren, K.J., Wilkinson, J., Miranda-Saksena, M., McInerney, G.M., Byth-Wilson, K., Robinson, P.J., Cunningham, A.L., 2010. A differential role for macropinocytosis in mediating entry of the two forms of vaccinia virus into dendritic cells. PLoS Pathog. 6, e1000866.
Sato, S., Trackman, P.C., Maki, J.M., Myllyharju, J., Kirsch, K.H., Sonenshein, G.E., 2011. The Ras signaling inhibitor LOX-PP interacts with Hsp70 and c-Raf to reduce Erk activation and transformed phenotype of breast cancer cells. Mol. Cell Biol. 31, 2683–2695.
Sato, S., Zhao, Y., Imai, M., Simister, P.C., Feller, S.M., Trackman, P.C., Kirsch, K.H., Sonenshein, G.E., 2013. Inhibition of CIN85-mediated invasion by a novel SH3 domain binding Motif in the lysyl oxidase propeptide. PloS One 8, e77288.
Schornack, P.A., Gillies, R.J., 2003. Contributions of cell metabolism and H+ diffusion to the acidic pH of tumors. Neoplasia 5, 135–145.
Shogomori, H., Futerman, A.H., 2001. Cholera toxin is found in detergent-insoluble rafts/domains at the cell surface of hippocampal neurons but is internalized via a raft-independent mechanism. J. Biol. Chem. 276, 9182–9188.
Sun, P., Yamamoto, H., Suetsugu, S., Miki, H., Takenawa, T., Endo, T., 2003. Small GTPase Rah/Rab34 is associated with membrane ruffles and macropinosomes and promotes macropinosome formation. J. Biol. Chem. 278, 4063–4071.
Tannock, I.F., Rotin, D., 1989. Acid pH in tumors and its potential for therapeutic exploitation. Cancer Res. 49, 4373–4384.
Tapper, H., Sundler, R., 1995. Bafilomycin A1 inhibits lysosomal, phagosomal, and plasma membrane H(+)-ATPase and induces lysosomal enzyme secretion in macrophages. J. Cell Physiol. 163, 137–144.
Thai, T.P., Rodemer, C., Jauch, A., Hunziker, A., Moser, A., Gorgas, K., Just, W.W., 2001. Impaired membrane traffic in defective ether lipid biosynthesis. Hum. Mol. Genet. 10, 127–136.
Tiruppathi, C., Song, W., Bergenfeldt, M., Sass, P., Malik, A.B., 1997. Gp60 activation mediates albumin transcytosis in endothelial cells by tyrosine kinase-dependent pathway. J. Biol. Chem. 272, 25968–25975.
Torgersen, M.L., Skretting, G., van Deurs, B., Sandvig, K., 2001. Internalization of cholera toxin by different endocytic mechanisms. J. Cell Sci. 114, 3737–3747.
Vora, S.R., Guo, Y., Stephens, D.N., Salih, E., Vu, E.D., Kirsch, K.H., Sonenshein, G.E., Trackman, P.C., 2010a. Characterization of recombinant lysyl oxidase propeptide. Biochemistry 49, 2962–2972.
Vora, S.R., Palamakumbura, A.H., Mitsi, M., Guo, Y., Pischon, N., Nugent, M.A., Trackman, P.C., 2010b. Lysyl oxidase propeptide inhibits FGF-2-induced signaling and proliferation of osteoblasts. J. Biol. Chem. 285, 7384–7393.
Wadia, J.S., Stan, R.V., Dowdy, S.F., 2004. Transducible TAT-HA fusogenic peptide enhances escape of TAT-fusion proteins after lipid raft macropinocytosis. Nat. Med. 10, 310–315.
Wang, H., Haas, M., Liang, M., Cai, T., Tian, J., Li, S., Xie, Z., 2004. Ouabain assembles signaling cascades through the caveolar Na+/K+-ATPase. J. Biol. Chem. 279, 17250–17259.
Wang, J.T.H., Teasdale, R.D., Liebl, D., 2014. Macropinosome quantitation assay. MethodsX 1, 36–41.
Wang, L., Sapuri-Butti, A.R., Aung, H.H., Parikh, A.N., Rutledge, J.C., 2008. Triglyceride-rich lipoprotein lipolysis increases aggregation of endothelial cell membrane microdomains and produces reactive oxygen species. Am. J. Physiol. Heart Circ. Physiol. 295, H237–H244.

Waugh, D.S., 2011. An overview of enzymatic reagents for the removal of affinity tags. Protein Expr. Purif. 80, 283–293.
Yoshimori, T., Yamamoto, A., Moriyama, Y., Futai, M., Tashiro, Y., 1991. Bafilomycin A1, a specific inhibitor of vacuolar-type H(+)-ATPase, inhibits acidification and protein degradation in lysosomes of cultured cells. J. Biol. Chem. 266, 17707–17712.
Yu, Z., Sato, S., Trackman, P.C., Kirsch, K.H., Sonenshein, G.E., 2012. Blimp1 activation by AP-1 in human lung cancer cells promotes a migratory phenotype and is inhibited by the lysyl oxidase propeptide. PloS One 7, e33287.
Zayzafoon, M., Abdulkadir, S.A., McDonald, J.M., 2004. Notch signaling and ERK activation are important for the osteomimetic properties of prostate cancer bone metastatic cell lines. J. Biol. Chem. 279, 3662–3670.
Zenni, M.K., Giardina, P.C., Harvey, H.A., Shao, J., Ketterer, M.R., Lubaroff, D.M., Williams, R.D., Apicella, M.A., 2000. Macropinocytosis as a mechanism of entry into primary human urethral epithelial cells by Neisseria gonorrhoeae. Infect. Immun. 68, 1696–1699.
Zhao, Y., Min, C., Vora, S.R., Trackman, P.C., Sonenshein, G.E., Kirsch, K.H., 2009. The lysyl oxidase pro-peptide attenuates fibronectin-mediated activation of focal adhesion kinase and p130Cas in breast cancer cells. J. Biol. Chem. 284, 1385–1393.
Zouwail, S., Pettitt, T.R., Dove, S.K., Chibalina, M.V., Powner, D.J., Haynes, L., Wakelam, M.J., Insall, R.H., 2005. Phospholipase D activity is essential for actin localization and actin-based motility in Dictyostelium. Biochem. J. 389, 207–214.